

SOLAREX CORP ROCKVILLE MD
SILICON SOLAR CELL OPTIMIZATION.(U)
JUN 80 J H WOHLGEMUTH, A L SCHEININE

F33615-78-C-2039

AFWAL-TR-80-2059

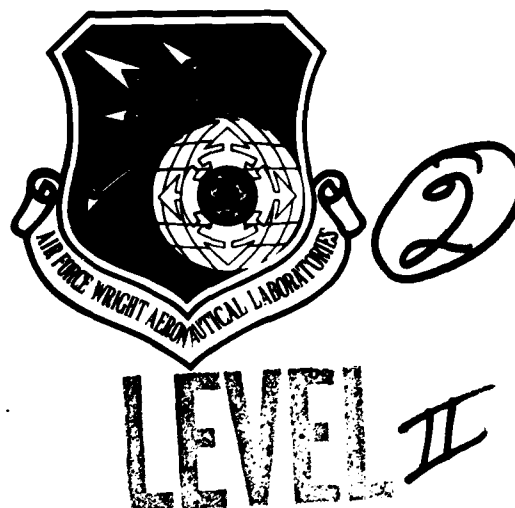
NL

1. 1000
2. 1000
3. 1000
4. 1000
5. 1000
6. 1000
7. 1000
8. 1000
9. 1000
10. 1000

END
DATE
FILMED
2-8
DTIC

AD A092908

AFWAL-TR-80-2059



SILICON SOLAR CELL OPTIMIZATION

SOLAREX CORPORATION
1335 PICCARD DRIVE
ROCKVILLE, MARYLAND 20850

DTIC
ELECT
DEC 11 1980
S E

JUNE 1980

TECHNICAL REPORT AFWAL-TR-80-2059
Interim Report for period August 1978 — February 1980

Approved for public release; distribution unlimited.

DDC FILE COPY

AERO PROPULSION LABORATORY
AIR FORCE WRIGHT AERONAUTICAL LABORATORIES
AIR FORCE SYSTEM COMMAND
WRIGHT-PATTERSON AIR FORCE BASE, OHIO 45433

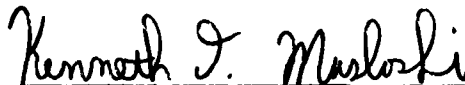
80 12 10 109

NOTICE

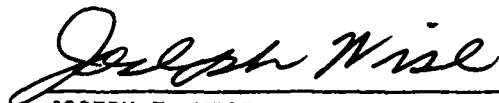
When Government drawings, specifications, or other data are used for any purpose other than in connection with a definitely related Government procurement operation, the United States Government thereby incurs no responsibility nor any obligation whatsoever; and the fact that the government may have formulated, furnished, or in any way supplied the said drawings, specifications, or other data, is not to be regarded by implication or otherwise as in any manner licensing the holder or any other person or corporation, or conveying any rights or permission to manufacture use, or sell any patented invention that may in any way be related thereto.

This report has been reviewed by the Office of Public Affairs (ASD/PA) and is releasable to the National Technical Information Service (NTIS). At NTIS, it will be available to the general public, including foreign nations.

This technical report has been reviewed and is approved for publication.

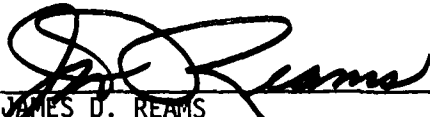


KENNETH T. MASLOSKI, 2Lt, USAF
Project Engineer
Energy Conversion Branch



JOSEPH F. WISE
TAM, Solar/Thermal Power
Energy Conversion Branch
Aerospace Power Division

FOR THE COMMANDER



JAMES D. REAMS
Chief, Aerospace Power Division
Aero Propulsion Laboratory

"If your address has changed, if you wish to be removed from our mailing list, or if the addressee is no longer employed by your organization please notify AFWAL/POOC-2 W-PAFB, OH 45433 to help us maintain a current mailing list".

Copies of this report should not be returned unless return is required by security considerations, contractual obligations, or notice on a specific document.

SECURITY CLASSIFICATION OF THIS PAGE (When Data Entered)

REPORT DOCUMENTATION PAGE		READ INSTRUCTIONS BEFORE COMPLETING FORM	
1. REPORT NUMBER AFWAL-TR-80-2059	2. GOVT ACCESSION NO. AD-A092 908	3. RECIPIENT'S CATALOG NUMBER	
4. TITLE (and Subtitle) SILICON SOLAR CELL OPTIMIZATION.		5. TYPE OF REPORT & PERIOD COVERED Interim Aug 1978 - Feb 1980	
7. AUTHOR(s) J. H. Wohlgemuth A. L. Scheinine		6. PERFORMING ORG. REPORT NUMBER	
9. PERFORMING ORGANIZATION NAME AND ADDRESS Solarex Corporation 1335 Piccard Drive Rockville, Maryland 20850		8. CONTRACT OR GRANT NUMBER(s) F33615-78-C-2039	
11. CONTROLLING OFFICE NAME AND ADDRESS Aero Propulsion Laboratory (AFWAL/POOC-2) AF Wright Aeronautical Laboratory, AFSC Wright-Patterson AFB, Ohio 45433		10. PROGRAM ELEMENT, PROJECT, TASK AREA & WORK UNIT NUMBERS	
14. MONITORING AGENCY NAME & ADDRESS (if different from Controlling Office)		12. REPORT DATE June 1980	
		13. NUMBER OF PAGES 68	
		15. SECURITY CLASS. (of this report) UNCLASSIFIED	
		15a. DECLASSIFICATION DOWNGRADING SCHEDULE	
16. DISTRIBUTION STATEMENT (of this Report) Approved for Public Release; Distribution Unlimited			
17. DISTRIBUTION STATEMENT (of the abstract entered in Block 20, if different from Report) Approved for Public Release; Distribution Unlimited			
18. SUPPLEMENTARY NOTES			
19. KEY WORDS (Continue on reverse side if necessary and identify by block number) Vertical Junction Solar Cells Silicon Solar Cells Solar Cells Space Photovoltaic Power			
20. ABSTRACT (Continue on reverse side if necessary and identify by block number) This research program has resulted in improvements in vertical junction solar cell techniques leading to higher efficiencies and improved handleability. Vertical junction solar cells have now been fabricated with AMO conversion efficiency greater than 15% (25°C). A variety of cells have been fabricated including different groove depths, substrate thicknesses and bulk resistivities. Cell performance has been measured both before and after			

DD FORM 1 JAN 73 1473

EDITION OF 1 NOV 65 IS OBSOLETE

SECURITY CLASSIFICATION OF THIS PAGE (When Data Entered)

312-12

-2

→ irradiation. Theoretical analysis has been performed to generate computer models of I-V curves for various cell geometries. These models have been compared with actual cell performance to aid in the understanding of the mechanisms responsible for cell performance. ↙

FORWORD

This Technical Report covers all work performed under Contract No. F33615-78-C-2039, entitled "Silicon Solar Cell Optimization". The effort was sponsored by the Aero Propulsion Laboratory, AF Wright Aeronautical Laboratories Air Force Systems Command, Wright-Patterson Air Force Base, Ohio under Project 3145. Mr. J. Beam (AFWAL/POOC) was the Air Force Project Engineer, while Dr. John Wohlgemuth of Solarex Corporation was technically responsible for the work.

The work reported herein was performed during the period 15 August 1978 to 15 January 1980.

The authors wish to thank Dr. Patrick Rahilly and Dr. George Storti for helpful suggestions and Mr. Donald Warfield, Ms. Eileen Sparks and Mr. R. Edwards for cell fabrication.

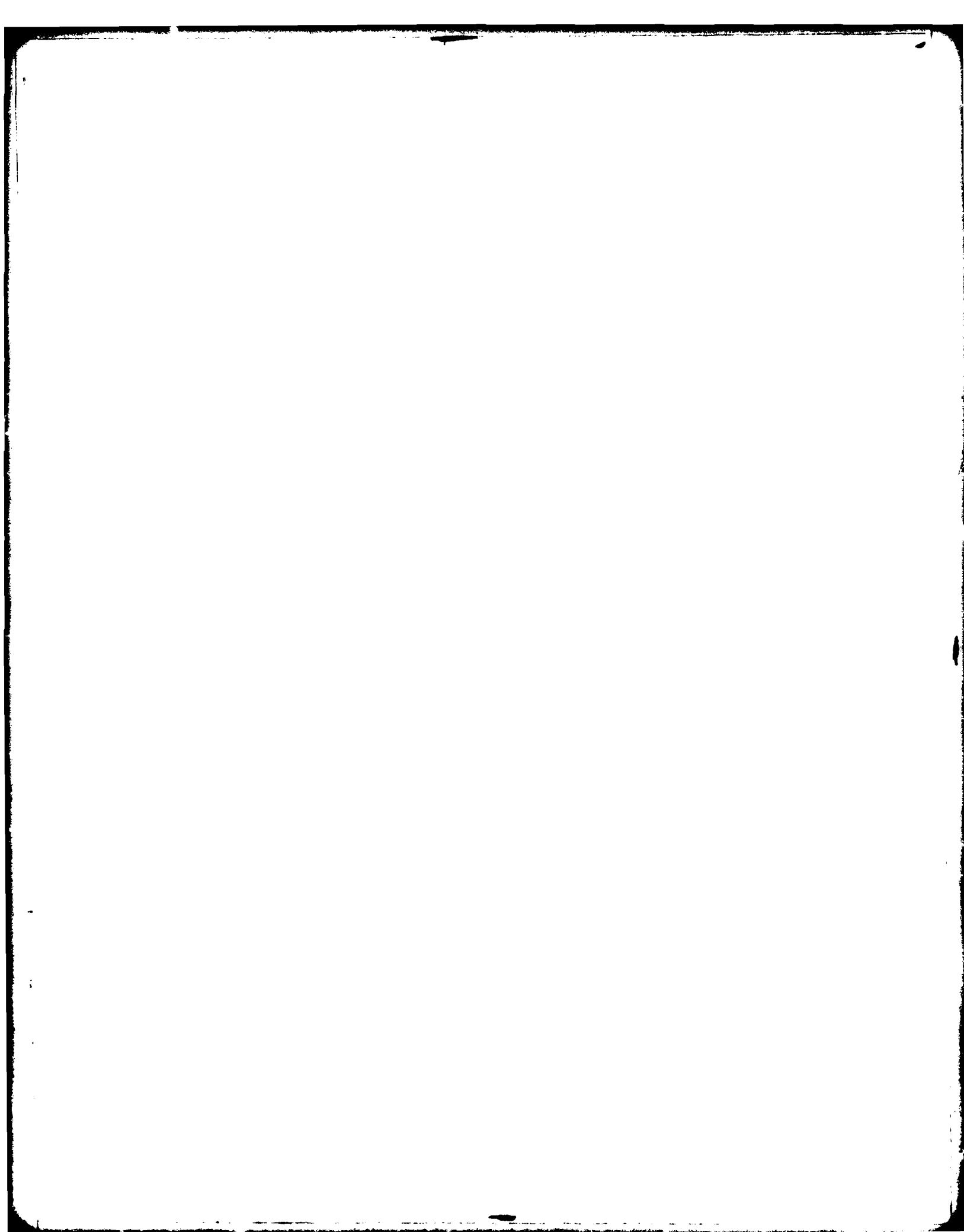


TABLE OF CONTENTS

SECTION	PAGE
1 INTRODUCTION	1
2 EXPERIMENTAL PROCEDURE	6
1. VJ Structure Formation	6
2. Cell Fabrication	13
3. Substrate Thinning	18
4. Coversliding	20
3 CELL MODELING	22
1. Theoretical Analysis	22
2. I-V Modeling	29
4 DEVICE PERFORMANCE	36
1. I-V Characteristics	37
2. AR Coatings	41
3. Radiation Resistance	49
4. Optical Characteristics	56
5. High Temperature Contact	61
5 CONCLUSIONS	65
REFERENCES	68

Accession For	
NTIS GR&I	<input checked="" type="checkbox"/>
DDC TAB	<input type="checkbox"/>
Unannounced	<input type="checkbox"/>
Justification	<input type="checkbox"/>
By _____	
Distribution/ _____	
Availability Codes	
Dist.	Avail and/or special
A	

LIST OF ILLUSTRATIONS

FIGURE		PAGE
1	Structure of Vertical Junction Solar Cell	2
2	SEM Pictures of Wall Rounding.....	10
3	Drawing of Mask Design	12
4	Reflectometer Graph of Wall Rounding	14
5	Flow Chart of Process Sequence	15
6	Photograph of 2 cm x 2 cm VJ Cell	19
7	I-V Characteristics of VJ Cell Before & After Thermal Cycling with Cover Attached	21
8	Lattice for Vertical Junction Solar Cell Modeling	23
9	Points Adjacent to $n_{i,j}$	28
10	Idealized I-V Curves as a Function of Minority Carrier Diffusion Length - Old Geometry	30
11	Idealized I-V Curves as a Function of Minority Carrier Diffusion Length - New Geometry	31
12	Idealized I-V Curves as a Function of Substrate Thickness for a Variety of Groove Depths	33
13	Angular Dependence of Short Circuit Current for Liquid AR Coatings	44
14	I-V Curve Before and After Filling the Grooves with Liquid Ta_2O_5	46
15	Reflection vs Wavelength for a Single Layer and Double Layer AR Coating on a VJ Cell	47
16	a. P/P_o vs Fluence for Various Substrate Thicknesses	50
	b. I_{sc}/I_{sco}	51
	c. V_{oc}/V_{oco}	52

FIGURE		PAGE
17	a. P/P_0 vs Fluence as a Function of Bulk Resistivity	53
	b. I_{sc}/I_{sco}	54
	c. V_{oc}/V_{oco}	55
18	a. P/P_0 vs Fluence as a Function of Groove Depth	57
	b. I_{sc}/I_{sco}	58
	c. V_{oc}/V_{oco}	59
19	P/P_0 vs Fluence for a Thin Shallow Groove 10 Ω -cm VJ Cell, a Thick Deep Groove 2 Ω -cm Cell, and a Planar Control 2 Ω -cm Cell	60

LIST OF TABLES

TABLE		PAGE
1	Continuous and Discrete Presentations of Boundary Conditions	28
2	Comparison of Computer Model Performance for Old and New Geometry Cells	35
3	Parameters of 15% Efficient VJ Cells	36
4	Performance of 15% Efficient VJ Cells at AM0 and 25°C	38
5	Thin-Substrate VJ Cells, Present Best Performance for 2 cm x 2 cm Cells	39
6	Comparison of Electrical Performance	41
7	Optical Properties of New-Geometry Cells with Ceria-Doped Covers	61

SECTION I

INTRODUCTION

The goal of this program is to improve the beginning-of-life (BOL) AM0 efficiency of silicon solar cells without sacrificing the radiation resistance so that a significant improvement in the end-of-life (EOL) efficiency can be obtained. Solarex has elected to use the vertical junction (VJ) cell structure for this program since it results in cells that are more radiation-resistant than other silicon structures. Therefore, improvements in BOL efficiency will result in higher EOL efficiency.

The vertical junction solar cell is made from a silicon slice with grooves etched into one surface. Grooves on the order of 5 microns wide spaced 15 to 20 microns apart are etched in the surface in a regular pattern. Figure 1 shows such a VJ structure. The diode junction follows the surface of the silicon up and down the walls. Since the walls are very narrow, carriers generated in the walls by incident light are always close to the collecting junction. Even if the carrier diffusion length is reduced, carriers created in the walls are able to traverse the short distance to the junction and be collected. Therefore, the

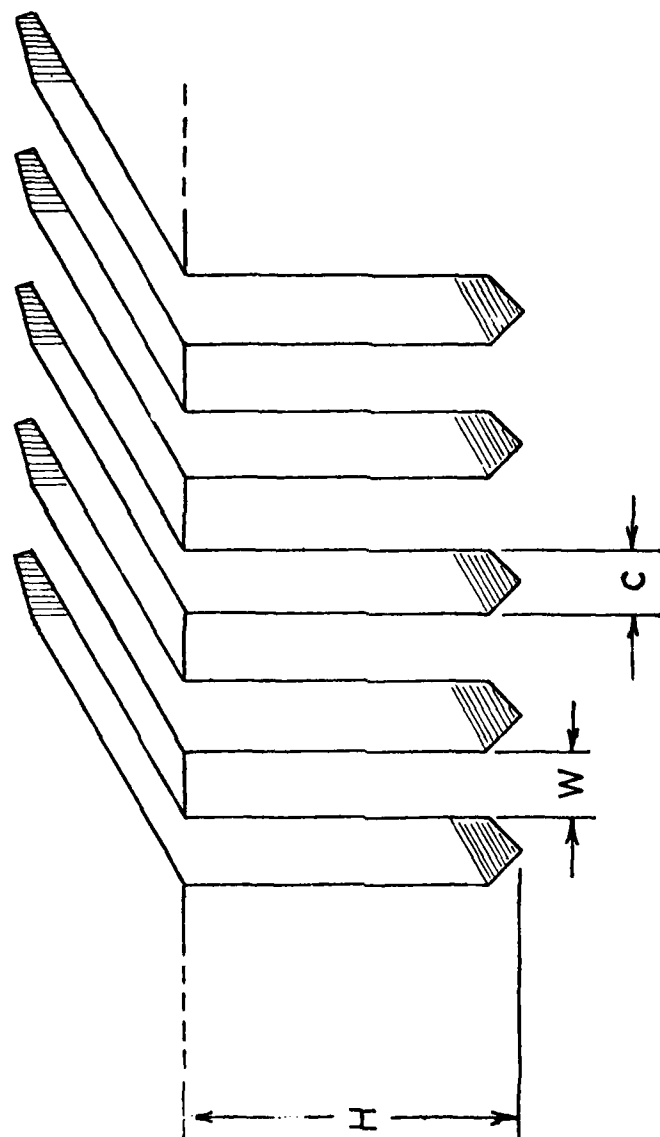


Figure 1: Structure of Vertical Junction Solar Cell

vertical junction cell has the inherent capability of providing superior radiation resistance.

During this phase of the effort, vertical junction cells have been fabricated with AM0 efficiencies greater than 15%. This improvement has been obtained by the use of new geometries, improved BSF formation and the use of double-layer AR coatings. The use of new cell geometries has enabled the fabrication of cell assemblies that can withstand thermal cycling and can be handled and connected by conventional techniques. These characteristics will allow VJ cells to be used in space arrays.

Thinning techniques have been employed to produce VJ cells with as little as 75 microns of silicon below the bottom of the grooves. This not only results in lightweight cells but improves the radiation resistance beyond that of a full-thickness VJ cell. This work has also shown that a highly polished silicon surface is not required for VJ fabrication: a standard chem-mechanical polish is adequate for the required photolithography.

The fabrication processes for VJ cells have been well documented in the literature (References 1 through 3). A brief description of the process techniques, with emphasis

on new developments or modifications, is presented in Section II. These new developments have simplified the process, providing for faster throughput and higher yields.

During this phase of the program, theoretical analysis has resulted in the development of computer-generated I-V curves for specific cell geometries and performance parameters. This modeling has aided in the evaluation of candidate cell structures and has identified important performance-limiting mechanisms. Comparison of theoretical and experimental performance has led to iterations in the modeling and identification of areas where the model does not correctly predict device performance. Section III describes the theory behind the model, the mathematics behind the computer programs and the predictions of the model for various cell structures.

The experimental results are described in Section IV. Characteristics of a variety of VJ structures are presented along with details of their performance after particulate irradiation. In addition, valuable information on cell assemblies such as optical performance and thermal cycling data are presented.

The final section summarizes the developments of this program to date and suggests the efforts to be undertaken to reach the intermediate goal of 16% AMO efficiency. It also assesses the effort required to reach the program goal of 18% BOL AMO efficiency.

SECTION 2

EXPERIMENTAL PROCEDURES

The techniques for formation of the vertical junction structure have been developed during previous efforts (References 1, 2, 4). During this program, modifications have been made to the process to improve cell performance, provide the structural integrity to withstand thermal cycling, simplify production requirements, and reduce cost and substrate thickness. The following sections describe (1) the formation of the VJ structure, (2) substrate thinning, (3) cell fabrication and (4) coverslide procedures.

1. VJ STRUCTURE FORMATION

The process which has made the vertical junction solar cell technically and economically feasible is the orientation-dependent etch. Kendall (Reference 5) found that the etch rate of silicon in KOH varies by a factor of up to 400 depending upon crystal orientation. The (111) plane of silicon is more resistant to the etch than the other crystal planes. Therefore, if silicon can be properly aligned and masked before etching, the required deep narrow grooves can be etched. If the silicon wafer is cut along the (110) plane, the (111) planes are normal to the surface. Aligning and etching this surface will

leave the vertical walls needed for the vertical junction cell.

Therefore, VJ cells must use (110) wafers. It is not practical to grow (110) ingots since this orientation cannot be grown dislocation-free. However, (110) wafers can be cut from either (111) or (100) ingots using x-ray alignment. A (111) flat must be cut on each wafer as an aid to later alignment during photolithography.

Because of the high-resolution photolithography required to define the narrow grooves for etching, the wafers must be smooth-surfaced. Initially, a highly polished surface was obtained using a cupric nitrate solution (Reference 6). However, it has now been found that citon etch and chemical polish etchants such as CP-etch leave a sufficiently smooth surface for the required photolithography.

Etching grooves into the silicon requires an effective alkaline etchant mask. This mask must be able to withstand the etching solution long enough that grooves of the required depth can be etched. In addition, the formation of the etchant mask must not degrade the silicon in any way. This has been accomplished by a

2-step process that includes a short heat treatment in the presence of a phosphorous atmosphere followed by the growth of oxide in steam, all at a temperature below 850°C.

The photolithography pattern must be aligned accurately to the (111) plane so that the orientation-dependent etch will produce deep, narrow grooves. To accomplish this, a flat mechanical stop is aligned optically to the photolithography mask. The wafers are then held against the stop while the resist is exposed.

The photoresist on the surface now acts as a mask for the oxide etch. The etchant is 6 NH_4F :1 HF . The etchant does not attack the photoresist or the silicon but does remove all of the oxide. Several minutes of etching removes the oxide from the windows with a minimum of undercutting.

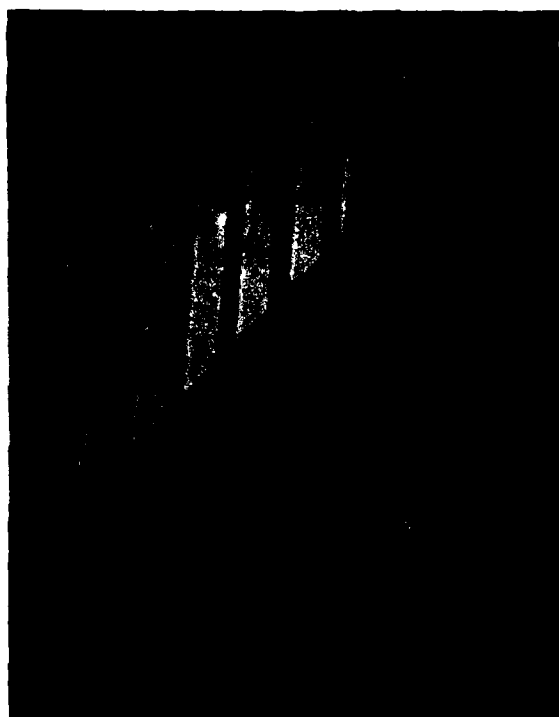
The orientation-dependent etchant found to yield the best results is 30% KOH in H_2O at 70° to 75°C. With this etchant, grooves 4 mils deep have been etched within one hour with a minimum increase in groove width. The resultant walls are extremely

straight and parallel with square tops as shown in Figure 2a.

The best radiation resistance requires maximum wall area under the constraint of keeping the junction within 5 to 10 microns of the core of the wall. It is therefore advantageous to etch the narrowest grooves possible. Etching experiments were conducted using photolithography mask openings ranging from 1 to 10 microns in width. The results indicated that the narrowest practical mask opening was 2.5 microns. This groove opening resulted in a final groove width (measured at the top) of approximately 5 microns for groove depths between 25 and 75 microns. This information was used to design a mask pattern with a groove opening of 2.5 microns and a step-and-repeat distance of 17.5 microns (Figure 3). This mask results in a VJ structure with grooves 5 to 6 microns wide and walls 12 to 13 microns wide.

After the orientation-dependent etch, the remainder of the masking oxide is removed with an HF etch.

Because of the "fake-diffusion" oxide growth, silicon from the wall tops must be removed. An acid etch containing a mixture of 1:3:8 (by volume) of 49% HF, 70% HNO_3 and 98% CH_3COOH is used to remove a small amount



Sample #C
Magnification: 720X



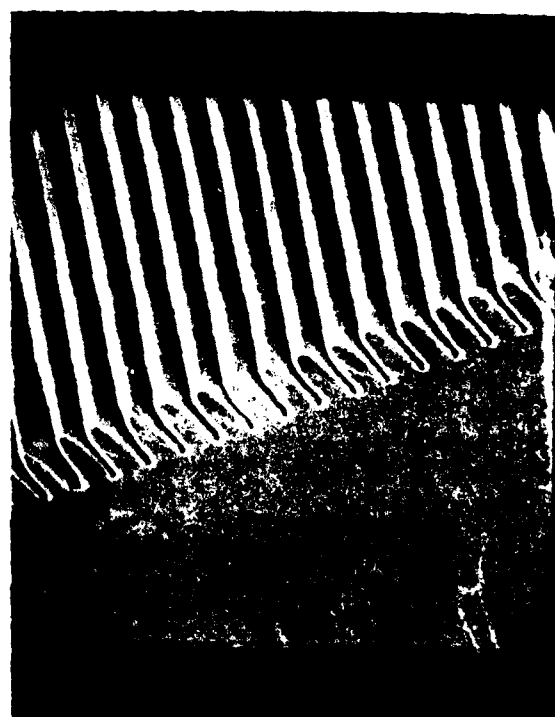
Sample #C
Magnification: 360X

Figure 2a.
No Texture Etch

Figure 2. SEM Pictures of Wall Rounding



Sample #60
Magnification: 720X



Sample #60
Magnification: 360X

Figure 2b.
After Texture Etch

Figure 2. Concluded

Not to Scale, All Values in Mils

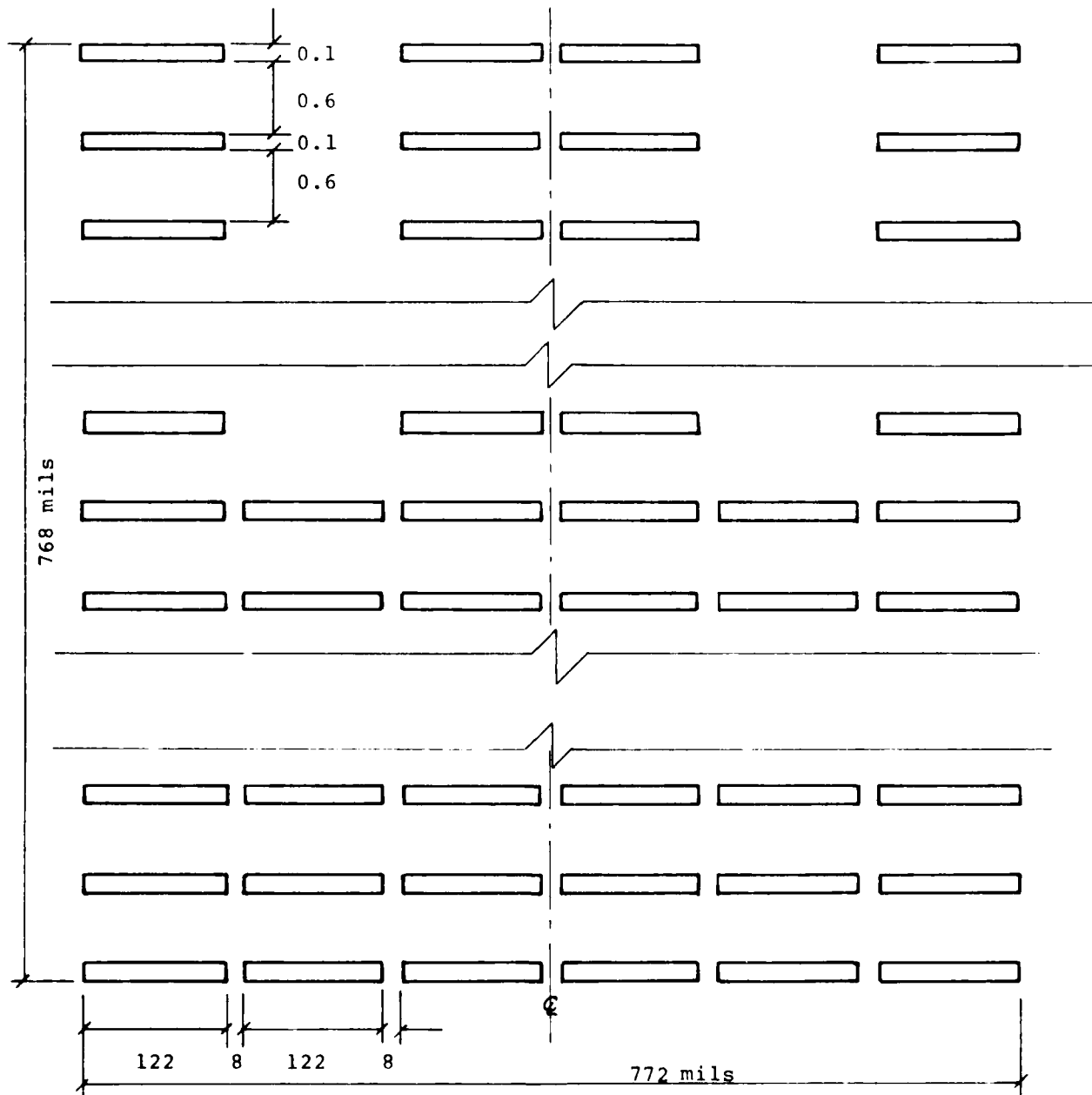


Figure 3. Drawing of Mask Design

of silicon. This etch rounds the wall tops and can be used to improve the optical absorption of the surface. Figure 2 illustrates the degree of rounding effected by etches of varying duration.

Although the more rounded walls provide better optical coupling (as shown in Figure 4), this structure has several disadvantages including (1) the increased groove area allows more of the light to impinge on the cell substrate rather than the wall, resulting in poorer radiation resistance, and (2) the narrower walls are more susceptible to breakage during thermal cycling. Therefore, a short etch (as shown in Figure 2b) has been employed for most cells, with improved optical coupling provided by alternate means (namely double-layer AR coating).

2. CELL FABRICATION

The orientation-dependent-etched silicon wafers are fabricated into solar cells by processes similar to those employed in the fabrication of planar cells. The unusual features of the vertical junction cell (e.g., exposure of multiple crystal planes and the need to diffuse down narrow grooves) have presented no substantial processing problems. The process sequence is shown in the flow chart in Figure 5. The various steps are described in the following subsections.

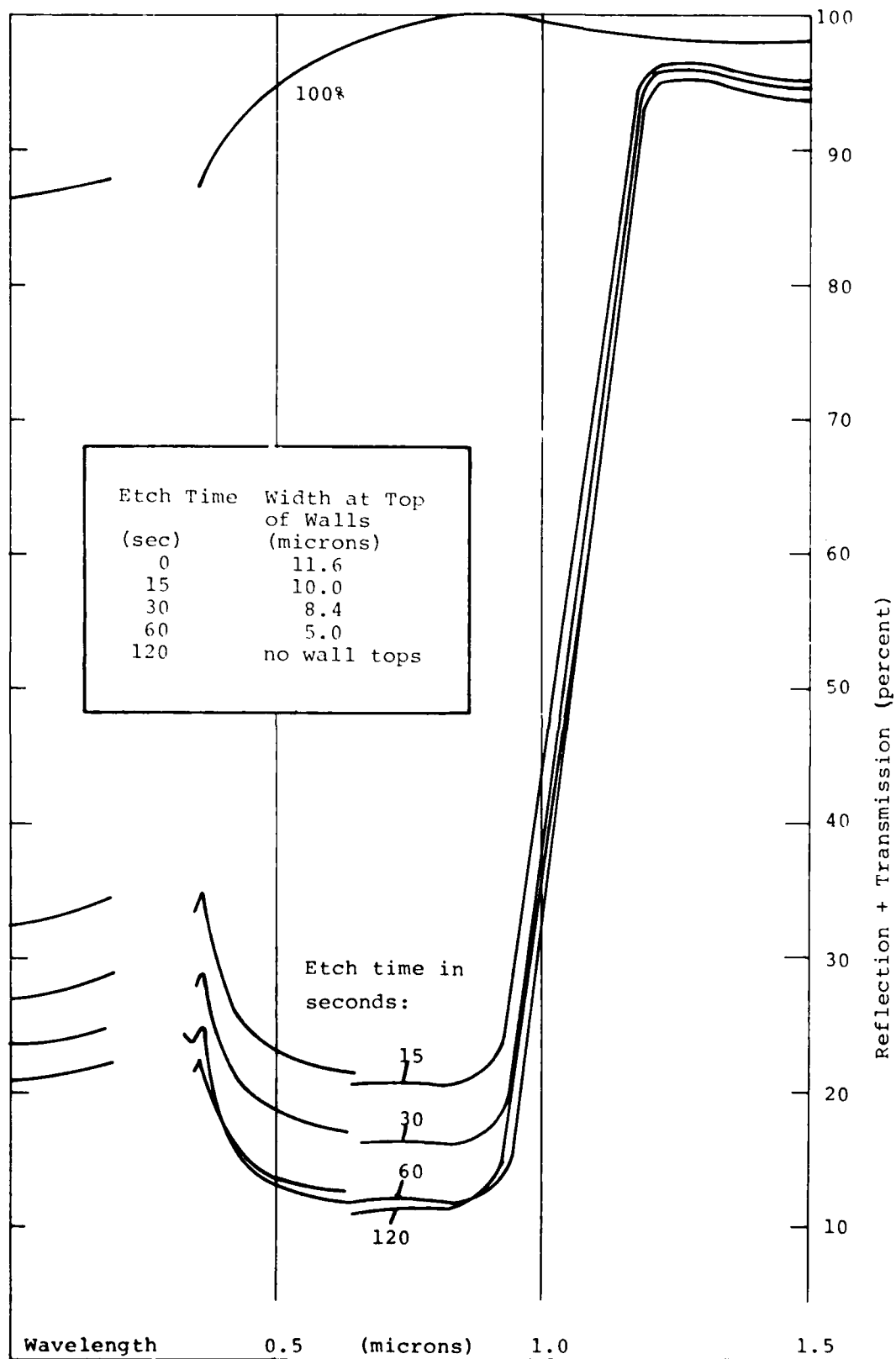


Figure 4. Reflectometer Graph of Wall Rounding

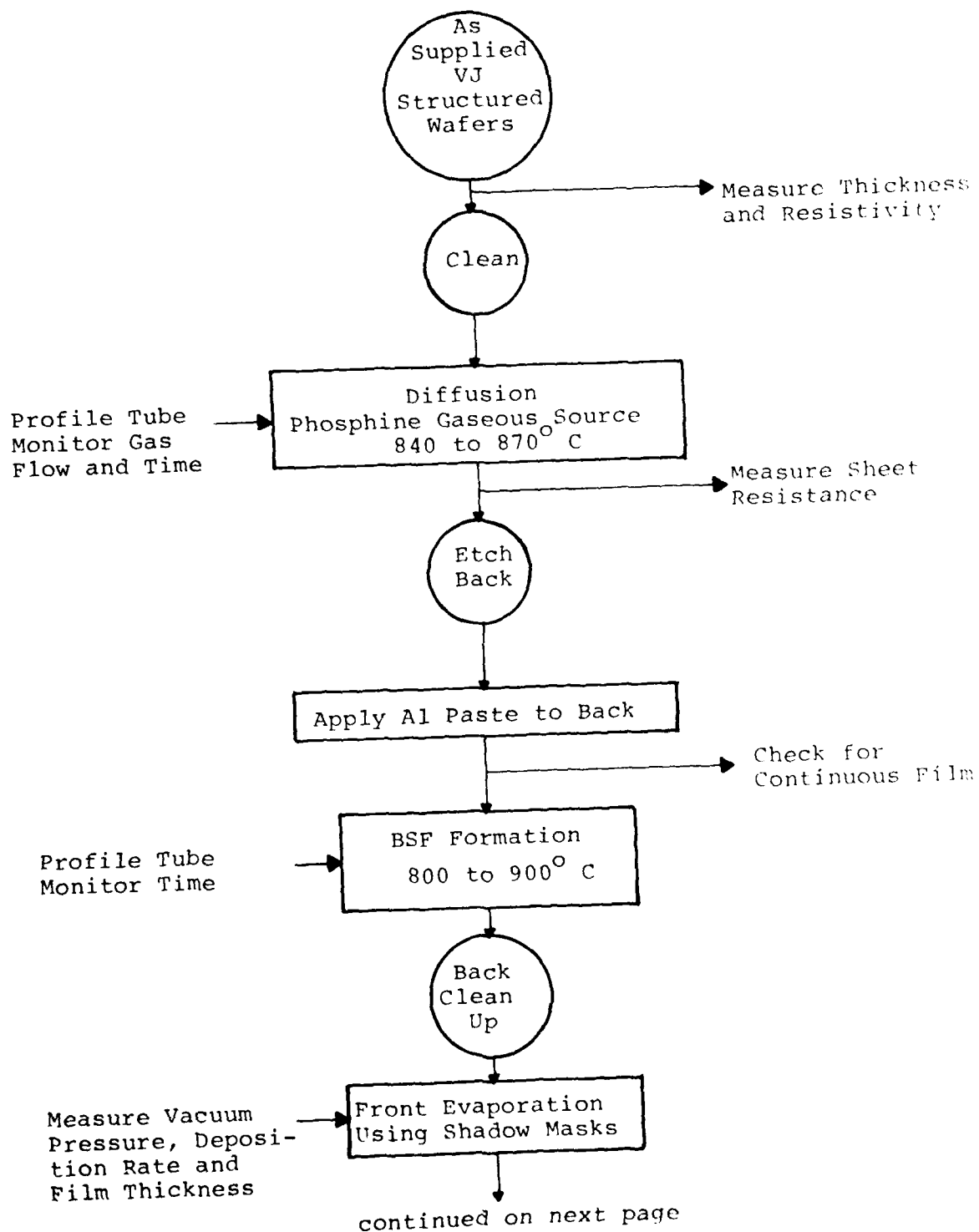


Figure 5. Flow Chart of Process Sequence

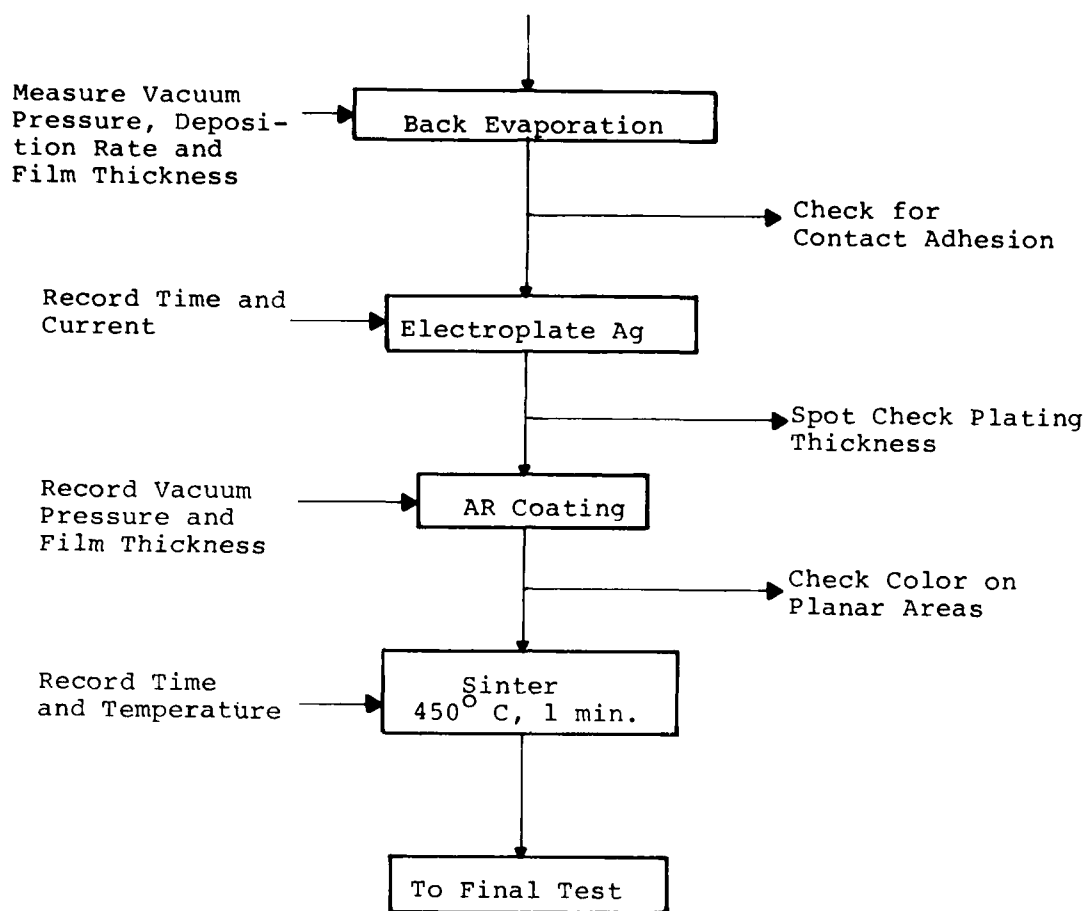


Figure 5. Concluded

a. Diffusion

The diffusion process is performed in a standard quartz diffusion tube with the wafers mounted in a quartz diffusion boat. The diffusion source is phosphine gas flowing through the tube. Diffusion temperatures between 840°C and 870°C have been utilized during a 12-to-16-minute diffusion cycle. The sheet resistance is checked on several samples to assure proper diffusion.

b. Al Paste BSF Formation

One of the major developments in cell processing has been the use of Al pastes for the formation of the back surface field. This technique results in a better BSF that provides a higher open-circuit voltage and improved long-wavelength response. One particular process technique has been developed for use with the Englehard paste #A-3484. The paste is screened onto the rear of the wafer with a 200-mesh screen. The paste is cured at 90°C for 30 minutes in air. Alloying is performed in a quartz diffusion tube in air. The entry, alloy and exit times are extremely short, with the entire process taking only a few minutes. Alloy temperatures between 800°C and 900°C have been employed, but the best results have been obtained with alloy temperatures close to the diffusion temperature. The resultant alloy products are removed by a hot HCl etch and rinse.

c. Contact Formation

The contacts are formed by vacuum evaporation of Ti-Pd and subsequent electroplating of Ag. The front metallization pattern is formed using shadow masks aligned so that the grid lines follow the ridges left for this purpose during etching. Plated Ag carries the current to the collection pads. A photograph of a 2 cm x 2 cm VJ cell is shown in Figure 6.

d. Anti-Reflective Coating

A variety of anti-reflective coatings has been used on the VJ cells including spun-on Ta_2O_5 and e-beam evaporated Ta_2O_5 , TiO_x , and double layers of $\text{Ta}_2\text{O}_5/\text{Al}_2\text{O}_3$, $\text{Ta}_2\text{O}_5/\text{MgF}_2$, $\text{TiO}_x/\text{Al}_2\text{O}_3$, and $\text{TiO}_x/\text{MgF}_2$. All of these materials have proven to be adequate AR coatings. The most efficient cells to date have been made using a $\text{TiO}_x/\text{MgF}_2$ double-layer AR coating. The results obtained using these AR coatings are presented in Section 4.

3. Substrate Thinning

The (110) silicon wafers can be thinned down by etching in CP26 containing a 3:5:6 (by volume) mixture of 49% HF, 70% HNO_3 and 98% of CH_3COOH . When properly activated, this etchant can remove the silicon at a rate of approximately 1 micron/second. This etching technique has been



Figure 6. Photograph of 2 cm x 2 cm VJ Cell

used to thin silicon wafers from the standard 10 to 12 mils down to as thin as 4 mils. The surface that results from the etch is smooth enough for the subsequent groove-defining photolithography. Indeed, this is a polishing etch; used directly on as-cut planar wafers, it results in surface texture adequate for photolithography.

4. COVERSLIDING

Ceria-doped glass cover slides have been attached to VJ cells using conventional Dow Corning silicone adhesives. Attention must be paid to outgassing of the grooves so that bubbles are not trapped in the adhesive. When covers were applied to the initial VJ cell design walls (5 - 8 microns thick with 75-micron-deep grooves), the assemblies could not withstand thermal cycling (reference NTS-II, Solarex & AFWAL in-house testing). Figure 7 shows the performance of covered VJ assembly before and after 5 cycles between -196°C and $+140^{\circ}\text{C}$. Visual inspection of these cells indicates that their walls crack during the thermal cycling. The new VJ structure walls (12 - 14 microns thick with 25-micron-deep grooves) have eliminated this problem. Cell assemblies using the new VJ structure have been subjected to up to 10 such thermal cycles without measureable change in output power. This new structure, therefore, has alleviated the coversliding problem without the need for developing new cover-slide techniques.

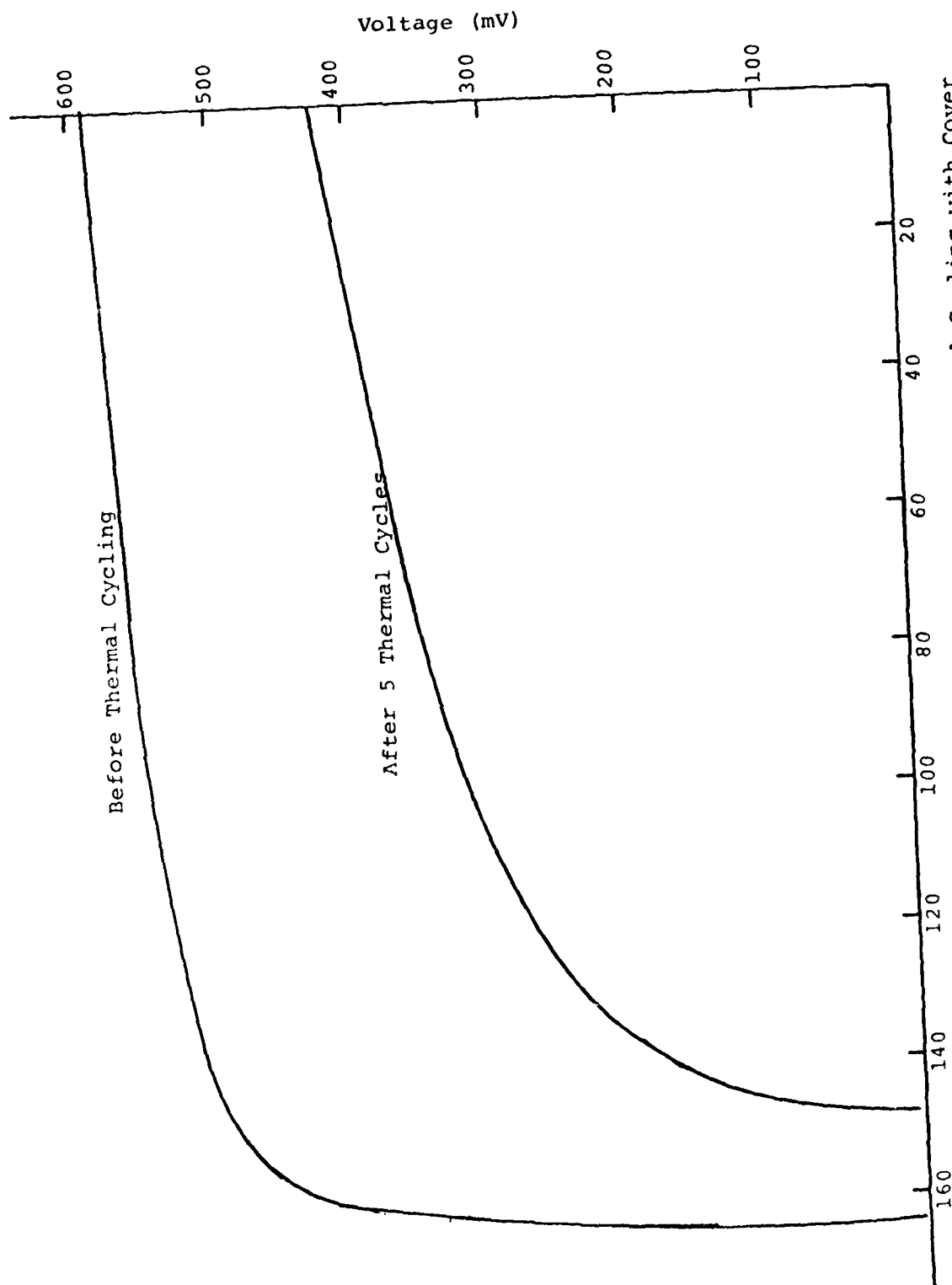


Figure 7. I-V Characteristics of VJ Cell Before and After Thermal Cycling with Cover Attached. 75 micron groove depth, 7 micron wall width.

SECTION 3

CELL MODELING

Typical first-order modeling of solar cell performance assumes a one-dimensional current flow. Because of its complex structure, the VJ cell requires the development of a two-dimensional current flow model. The approach taken to develop the model is to (1) define the appropriate equations and boundary conditions for carrier concentration at every point in the cell, (2) develop a numerical technique to solve the set of equations, (3) employ a computer to perform the numerical analysis, and (4) find the current that such a carrier distribution would predict. Details of the approach and the results for a variety of VJ cell structures and parameters are given in the following sections.

1. THEORETICAL ANALYSIS

The geometry of the VJ structure to be considered in the model is shown in Figure 8. A number of simplifying assumptions have been made:

1. The n^+ and p^+ regions are so thin that any carrier generation in these regions can be neglected.

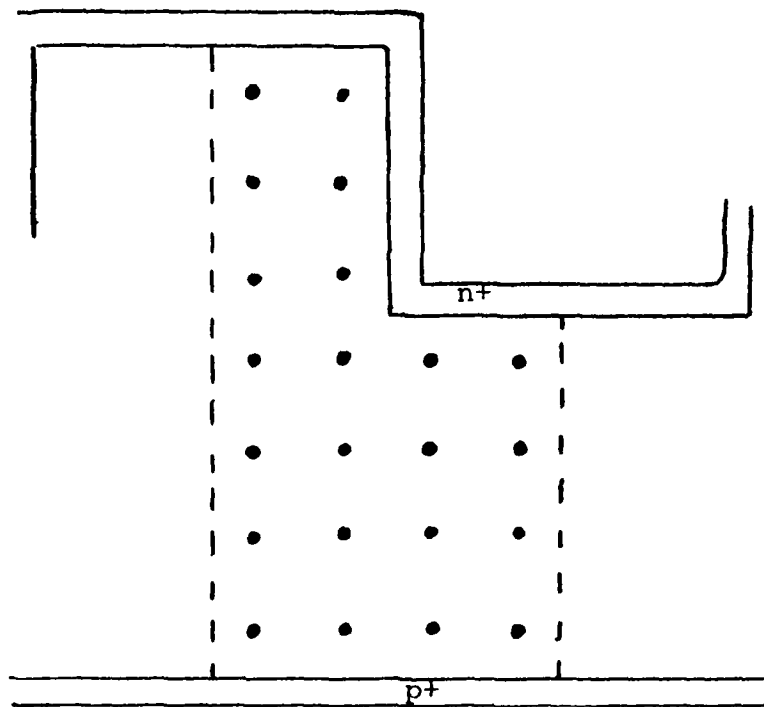


Figure 8. Lattice for Vertical Junction Solar Cell Modeling

2. The concentration of light-generated minority carriers in the p region is much denser than the equilibrium concentration of these minority carriers.
3. The electric field is confined to the depletion region and can be ignored in the bulk p region.

In the bulk p region the diffusion equation can then be written:

$$\nabla^2 n + G/D - n/L^2 = 0 \quad (1)$$

where n = free electron density in p-type silicon, excess above equilibrium value.

G = carrier generation rate due to illumination

D = diffusion constant

L = diffusion length of minority carrier

The following boundary conditions have been used:

- at the n^+/p front junction:

$$n = n_0 \exp (Vq/kT). \quad (2)$$

- at the p-p+ back junction there is a given surface recombination velocity such that:

$$\nabla n = nV_s/D. \quad (3)$$

- at the symmetry boundaries designated by surfaces C and D in Figure 8, the net flow of minority carriers is zero:

$$\nabla n = 0. \quad (4)$$

This set of differential equations must be solved to determine values of the minority carrier concentration at all points within the bulk. Then the current density can be determined by solving for the current density given by:

$$\vec{J} = qD\nabla n. \quad (5)$$

The value of the current density as a function of position along the n^+/p junction boundary must be found and the cell current determined by integrating over the junction surface. This technique is applicable to VJ cells at Air Mass Zero, but may not be applicable at higher concentrations when the current in the bulk generates an electric field that significantly modifies the diffusive flow.

To solve the set of equations a numerical technique, the relaxation method, has been implemented as a computer program. In the relaxation method the region is divided into discrete points and the equations are written in

terms of nearest-neighbor values. Figure 9 indicates the type of labeling used for a particular point and its adjacent neighbors. At point $n_{i,j}$ the diffusion equation can then be written:

$$\begin{aligned} & (n_{i+1,j} + n_{i-1,j} - 2n_{i,j}) / \Delta x^2 \\ & + (n_{i,j+1} + n_{i,j-1} - 2n_{i,j}) / \Delta y^2 \\ & + G_{i,j}/D - n_{i,j}/L^2 = 0 \end{aligned} \quad (6)$$

The determination of the generation rate, G , is based on an algorithm that is repeated eight times. Two parameters -- the absorption coefficient and the incident photon density -- are changed each time the algorithm is repeated. In this manner the air mass zero generation rate is approximated by summing the results of eight discrete cases. The algorithm traces both a vertical and a horizontal light path. In either case the generation rate is increased at a lattice point based on the amount of light extinguished when passing through the silicon surrounding that point.

The vertical path begins at the wall top and at the groove bottom, and is traced until reaching the back of the cell. The photon density of the vertical ray at the groove bottom is reduced from the full incident value by a certain fraction which is assigned, in turn, to the horizontal component. The horizontal component has a photon density equivalent to having the light spread across the entire groove wall.

The horizontal light path makes four transits across the groove walls, then the light path moves vertically through the silicon below the grooves. The four transits represents the fact that light makes several transits across a wall whether it is internally reflected or exits the wall and enters the adjacent wall.

At a boundary at least one of the adjacent points is outside the lattice. The boundary conditions are used to derive a value for this external point so that the value of the center point can be calculated as usual. Table 1 shows that, for the junction, the carrier density is an exponential function of voltage; for a fixed recombination velocity, the external point carrier density is a linear decrement of the central point value; and for the lines of symmetry, the external and center values are equal.

Equation 6 can be solved for $n_{i,j}$ so that the carrier density at the center point can be derived from the four adjacent points in a way that is consistent with the diffusion equation. The entire lattice is reconciled this way, constituting one computer cycle. The carrier

Table 1
CONTINUOUS AND DISCRETE REPRESENTATIONS OF BOUNDARY CONDITIONS

	Continuous	Discrete
Boundary Condition at Junction	$n = n_o e^{Vq/kT}$	$n_e = n_J = n_o (e^{Vq/kT} - 1)$
Boundary Condition for Surface with Recombination Velocity, V_s	$\nabla n = nV_s/D$	$n_e = n_{i,j} (1 - (\Delta r V_s/D))$
Zero Current Boundary	$\nabla n = 0$	$n_e = n_{i,j}$
Current at Junction	$\vec{J} = qD\nabla n$	$J = (n_{i,j} - n_J)qD/\Delta r$

where n_e = carrier density at an external point
 n_J = carrier density at junction
 Δr = Δx or Δy depending on the direction of displacement of two points

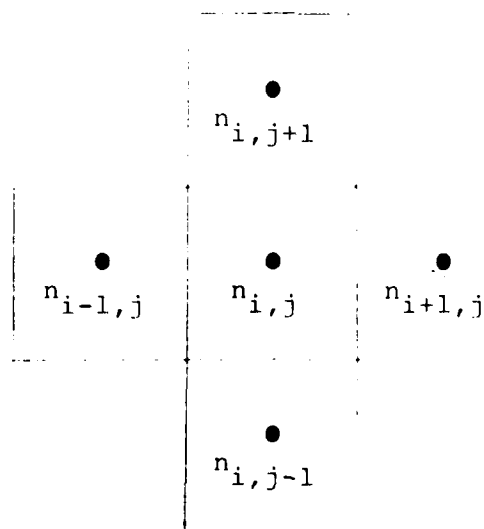


Figure 9. Points Adjacent to $n_{i,j}$

distribution converges to a steady state after several hundred cycles.

2. I-V MODELING

This computer model has now been employed to generate idealized (no series or shunt resistance included) I-V curves for a variety of VJ structures using various materials characteristics. Figure 10 shows the effect of diffusion length on the I-V curves for one particular cell structure, namely the old geometry with 7.5-micron-wide grooves and 7.5-micron-wide walls. The curves are plotted for 25-micron and 75-micron-deep grooves. Figure 11 shows the effect of diffusion length on the I-V curves for the new geometry with 12.5-micron-wide walls and 5.0-micron-wide grooves. The curves are plotted for 25-micron and 75-micron-deep grooves. Table 2 compares the two geometries. The new geometry results in slightly higher efficiencies as long as the diffusion length is longer than the wall thickness.

These curves (Figures 10 and 11) shows that:

- short-circuit current increases with increasing groove depth
- open-circuit voltage decreases with increasing groove depth.

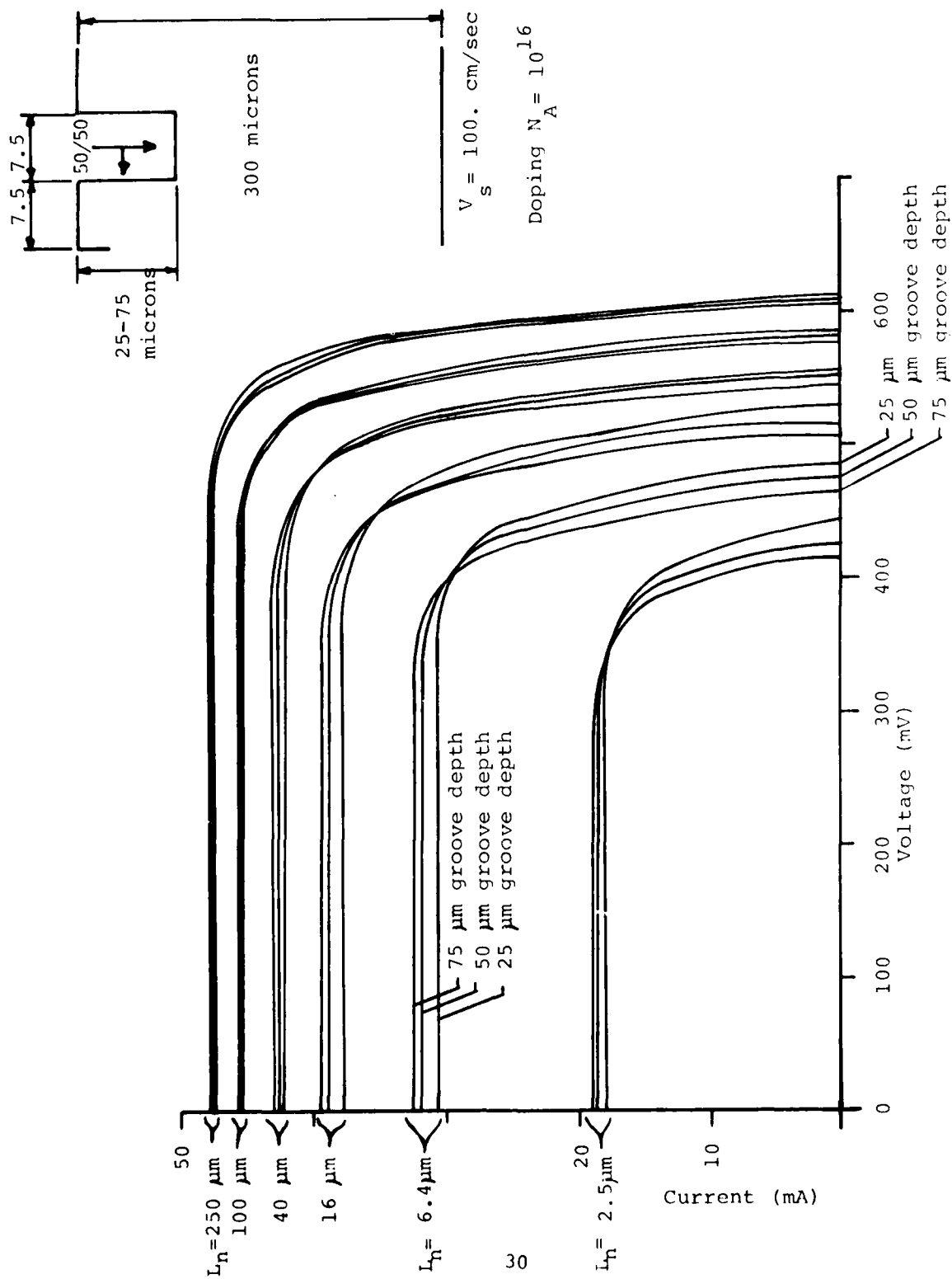


Figure 10. Idealized I-V Curves as a Function of Minority Carrier Diffusion Length - Old Geometry

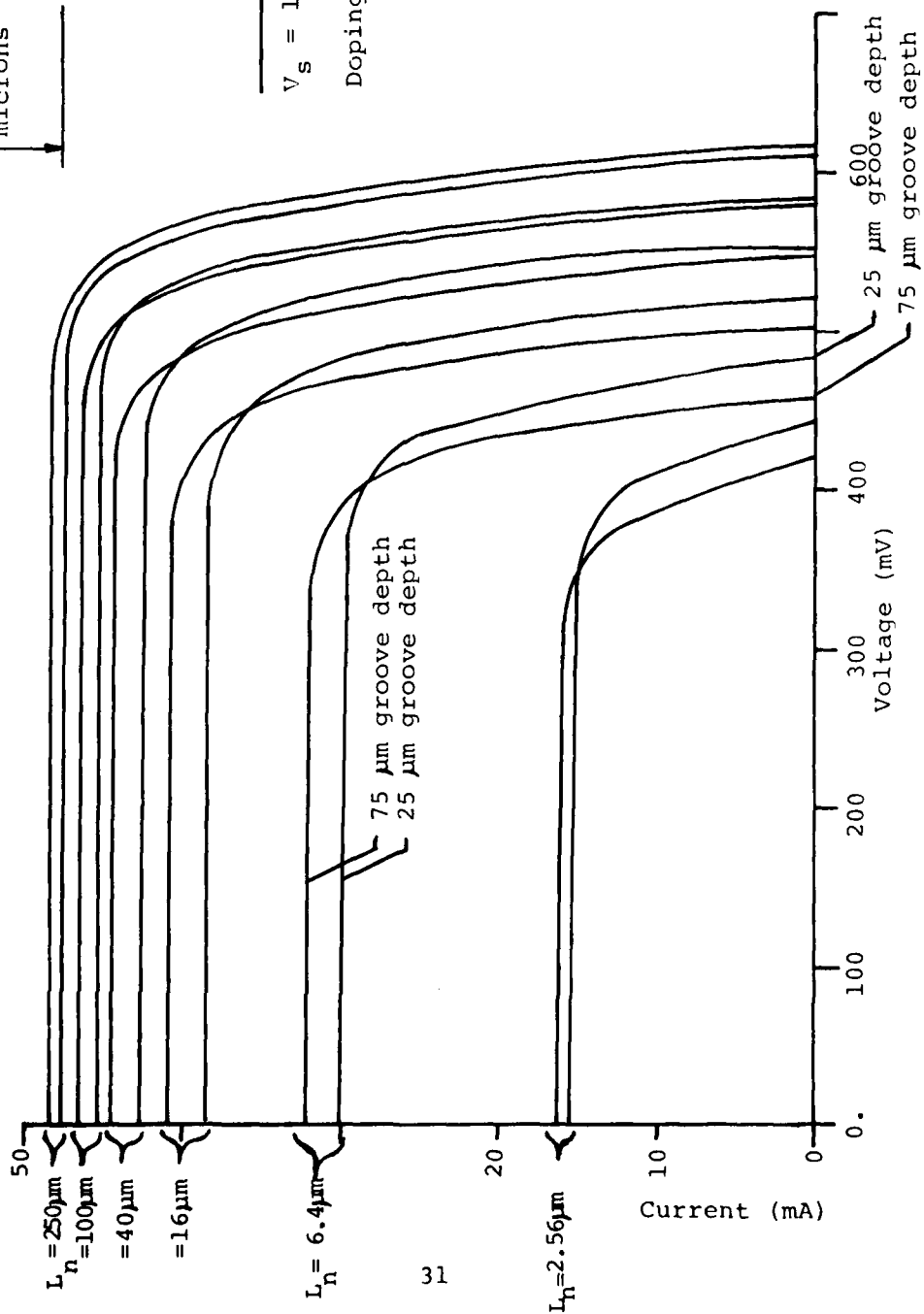
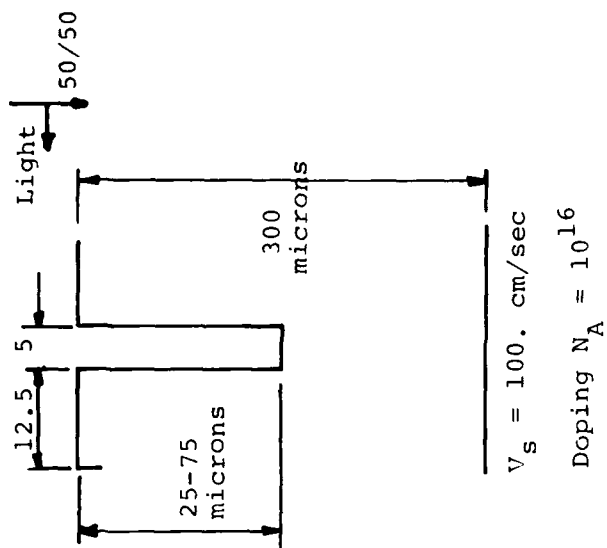


Figure 11. Idealized IV Curves as a Function of Minorities Carrier Diffusion Length - New Geometry

These observations agree with the experimental results given in Section 4. However, according to these computer-generated curves, the maximum power is insensitive to the groove depth for a given diffusion length. This has been verified for cells with long diffusion lengths (before irradiation) but, as is shown in Section 4., the cells with deeper grooves are appreciably more radiation-resistant than those with shallow grooves. This discrepancy may be because the model assumed optical coupling is independent of groove depth. In reality, the deeper the grooves, the more light enters the walls. A more accurate optical coupling model is now being developed.

Another parameter that has been investigated using the computer model is the effect of the substrate thickness on cell performance. Figure 12 shows the effect of substrate thickness on the I-V curves of new-geometry cells with 25-micron-deep grooves. For long diffusion lengths, the thicker cells have higher current and lower voltage. The model predicts that as diffusion length is reduced, the differences between cells of varying substrate thickness disappear. The experimental results, however, indicate that while current does perform as predicted, voltage does not: the cell voltages are independent of substrate thickness. Therefore, thinner substrates result in cells with lower BOL efficiency but with improved radiation resistance.

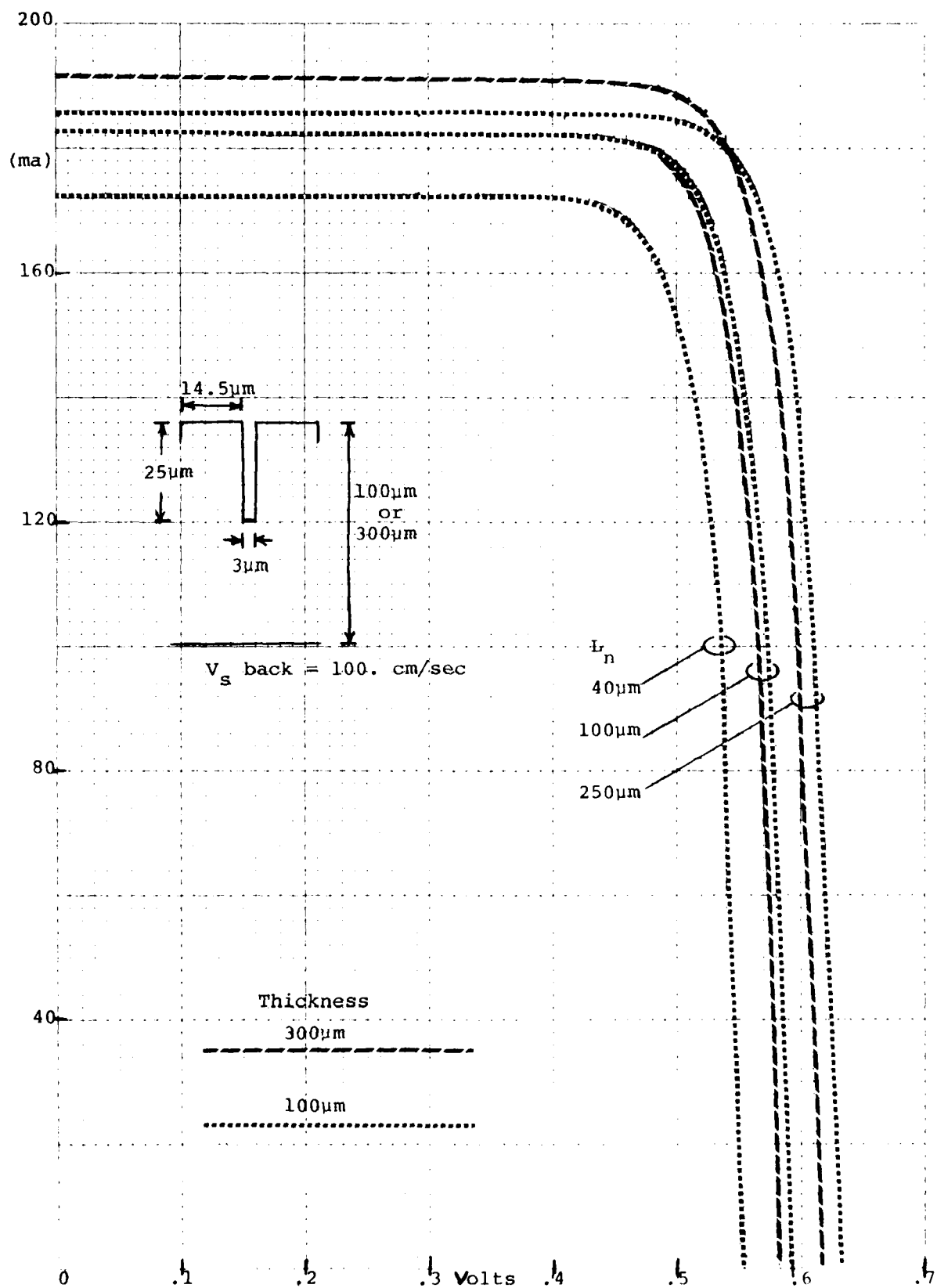


Figure 12. Idealized IV Curves as a Function of Substrate Thickness for a Variety of Groove Depths

The discrepancy between the model and the experimental results appears to be due to the effect of the BSF. In all probability, BSF cannot be modeled using a constant back surface recombination velocity. The BSF is an active junction and its performance can be affected by particulate irradiation. The computer model is now being modified to include an active $p-p^+$ junction in an effort to correctly model the dependence on substrate thickness.

The development of the two-dimensional computer model has aided in the understanding and development of new VJ structures. It has also indicated areas in which future efforts are required to complete our understanding of the mechanisms controlling cell performance. It is hoped that continued effort in these areas will lead to improvements in the design and performance of VJ cells.

Table 2
COMPARISON OF COMPUTER MODEL PERFORMANCE
FOR OLD AND NEW GEOMETRY CELLS

75 Micron Deep Grooves
2 μ -cm Silicon
300 Micron Thick Substrates

For 2 cm x 2 cm Cell

Diffusion Length		Old Geometry 7.5 μ -7.5 μ	New Geometry 12.5 μ -5.0 μ
250	P _{max}	98	98 mW
	I _{sc}	191	194 mA
	V _{oc}	609	616 mV
100	P _{max}	88	89 mW
	I _{sc}	183	186 mA
	V _{oc}	585	580 mV
40	P _{max}	77	78 mW
	I _{sc}	172	178 mA
	V _{oc}	550	546 mV
16	P _{max}	64	66 mW
	I _{sc}	158	164 mA
	V _{oc}	510	505 mV
6.4	P _{max}	47	47 mW
	I _{sc}	130	128 mA
	V _{oc}	460	460 mV
2.56	P _{max}	25	21 mW
	I _{sc}	77	65 mA
	V _{oc}	420	422 mV

SECTION 4

DEVICE PERFORMANCE

Vertical junction solar cells have been fabricated with AMO efficiencies in excess of 15%. Several different structures have been utilized to reach this power level. Table 3 summarizes the materials and structural parameters of the cells that have achieved the 15% efficiency level.

Table 3
Parameters of 15%-Efficient VJ Cells

Base Silicon:	P Type, Boron Doped 110 Orientation CZ Growth 10 to 12 Mils Thick 2 Ω -cm Resistivity
Processing:	Gaseous Phosphorous Diffusion Al Paste BSF Ti-Pd-Ag Front and Back TiO ₂ - MgF ₂ AR Coating
Geometry:	17.5 Microns Step and Repeat 2.5-Micron Groove Openings \approx 5.0-Micron-Wide Grooves 25- and 75-Micron-Deep Grooves Cells 2 cm x 2 cm

The I-V characteristics of these cells, including a discussion of the dependence of cell performance on various geometries, structures, and parameters are described in Section 4.1. Section 4.2 discusses the results of a variety of AR coating experiments. Section 4.3 details the results of radiation testing, while Section 4.4 describes the optical characteristics of these cells. Finally, Section 4.5 deals with the subject of high-temperature contacts for solar cells.

1. I-V CHARACTERISTICS

The performance parameters of two 15%-efficient VJ cells using two differing geometries are given in Table 4. From these values, several important observations can be made:

- The high current densities show that there is excellent light coupling into these VJ cells. As predicted by the modeling, deeper grooves result in higher currents.
- The open-circuit voltages for VJ cells are somewhat lower than can be obtained for similarly processed planar 2 Ω -cm silicon cells, which typically exhibited open-circuit voltages in the range of 610 to 620 mV. As one would expect from their larger junction area, the deeper-grooved cells have a lower voltage than the shallow-grooved cells.

Table 4

Performance of 15% Efficient VJ Cells
at AM0 and 25°C

25-Micron-Deep Grooves

I_{sc}	=	175 mA	
V_{oc}	=	597 mV	
Max P	=	82 mW	(15.1%)
I_{sc} Blue	=	48 mA	Corning #9788
I_{sc} Red	=	91 mA	Corning #2408
FF	=	78.5%	

75-Micron-Deep Grooves

I_{sc}	=	177 mA	
V_{oc}	=	583 mV	
Max P	-	82 mW	(15.1%)
I_{sc} Blue	-	49 mA	Corning #9788
I_{sc} Red	=	92 mA	Corning #2408
FF	=	79.5%	

- The fill factors are comparable with other high-efficiency silicon solar cells, showing that the metallization design is adequate. There is some indication that the shallow-groove cells are affected more by series resistance, due to their smaller silicon surface being required to carry the same total current. It may become necessary to redesign the shallow-groove metallization pattern somewhat, especially if higher currents are to be obtained from these cells.

Using the thinning techniques reported in Section 3, VJ cells on substrates as thin as 75 microns have been fabricated. Table 5 lists the maximum power obtainable to date for a variety of substrate thicknesses. It should be noted that the 125- and 75-micron-thick cells reported here had only a single-layer AR coating, while the thicker cells had a double-layer coating. It is estimated that with similar processing, only a few milliwatts will separate the thick and the thin cells.

Table 5
Thin-Substrate VJ Cells
Present Best Performance for 2 cm x 2 cm Cells

Thickness of Silicon (Microns)	P_{\max} (mW) at AM0
250	82
175	80
125	74
75	73

To compare the effects of groove depth, substrate thickness and bulk resistivity, an experiment was conducted. Using identical processing, cells were fabricated of 2 Ω -cm and 10 Ω -cm silicon using 250-micron and 175-micron-thick wafers and etching 25-, 50- and 75-micron-deep grooves. The results are shown in Table 6. The following observations can be made:

- Short-circuit current is nearly insensitive to bulk resistivity.
- Short-circuit current decreases with decreasing substrate thickness.
- Open-circuit voltage decreases with increasing bulk resistivity.
- Open-circuit voltage is unaffected by substrate thickness.
- Open-circuit voltage decreases with increasing groove depth.

These results indicate that the BSF does not reduce the back surface recombination velocity to as low a value as was assumed in the model described in Section 3.

Table 6
Comparison of Electrical Performance

Thickness	Resist. (ohm-cm)	Groove Depth→ (Microns)	\bar{I}_{sc} (mA)			\bar{V}_{oc} (mV)			\bar{P}_{max} (mW)		
			25	50	25	25	50	75	25	50	75
250 Microns	2		173	172	175	596	586	577	81	79	78
	10		172	172	173	585	576	572	78	78	77
175 Microns	2			158	168		585	578		74	75
	10		164	168	165	578	574	565	73	74	72

This experiment is continuing: a set of cells using 125-micron-thick substrates is now being fabricated. In addition, the model is being re-evaluated to determine a correct model for the BSF.

2. AR COATINGS

A variety of antireflective coatings have been employed on VJ cells. The evaporated layers are applied perpendicular to the surface (as for a planar cell) and the current increase is consistent with that expected as a result of the increase in absorption of the planar areas. The liquid AR coating results in a thicker coating on the walls and improves the current collected for non-perpendicular illumination. The following subsections describe the various AR coating results.

a. Single-Layer Vacuum-Evaporated Ta_2O_5

This is the standard space-quality quarter-wavelength AR coating, with an index of refraction of 2.05 to 2.2. The amount of current increase depends upon the geometry of the VJ cell and is consistent with the presence of this AR coating on the planar areas, and with 100% absorption of light that enters the grooves. With this AR coating there is still a minimum current loss of 6.1% due to reflection. In addition, we have observed a loss of open-circuit voltage upon application of the Ta_2O_5 coating. It is believed that this is due to an increased front surface recombination velocity caused by our particular technique for deposition of the Ta_2O_5 . While all early VJ cells were fabricated using a single-layer Ta_2O_5 AR coating, more recent cells have used either TiO_x single layers or multi-layer AR coatings.

b. Single-Layer Vacuum-Evaporated TiO_x

TiO_x is also a standard space-quality quarter-wavelength AR coating with an index of refraction of 2.0 to 2.2. Once again, the amount of current increase of VJ cells using it is consistent with its presence on the planar areas and with 100% absorption of light that enters the grooves. Since it is only a single-layer AR coating, there is still a minimum

current loss of 6.1% due to reflection. However, there is an increase in open-circuit voltage upon application of the TiO_x . Therefore, recent samples have utilized TiO_x rather than Ta_2O_5 .

c. Liquid Ta_2O_5

A commercially available Ta_2O_5 liquid AR material was obtained from Allied Chemical Corporation. The liquid coatings have been applied to VJ cells by spinning, spraying and dunking. The absorption of coated cells was improved over bare cells with each of these methods, but none of the liquid AR coatings were as good as the best evaporated Ta_2O_5 AR coatings. There is some evidence that the liquid AR does increase absorption in the sides of the walls, however. Figure 13 shows the short-circuit current of a VJ cell with liquid AR coating as a function of angle of incidence. As can be seen, the current is a maximum at an angle 15° from normal. Vacuum-evaporated AR coated cells have exhibited this phenomenon only after irradiation. It is therefore possible that the liquid AR will increase the fraction of light absorbed in the walls and therefore improve the radiation resistance of the cells.

Finally, in an attempt to develop a coversliding technique for VJ cells, liquid AR material was used to fill in the grooves. The cells, however, suffered severe loss in

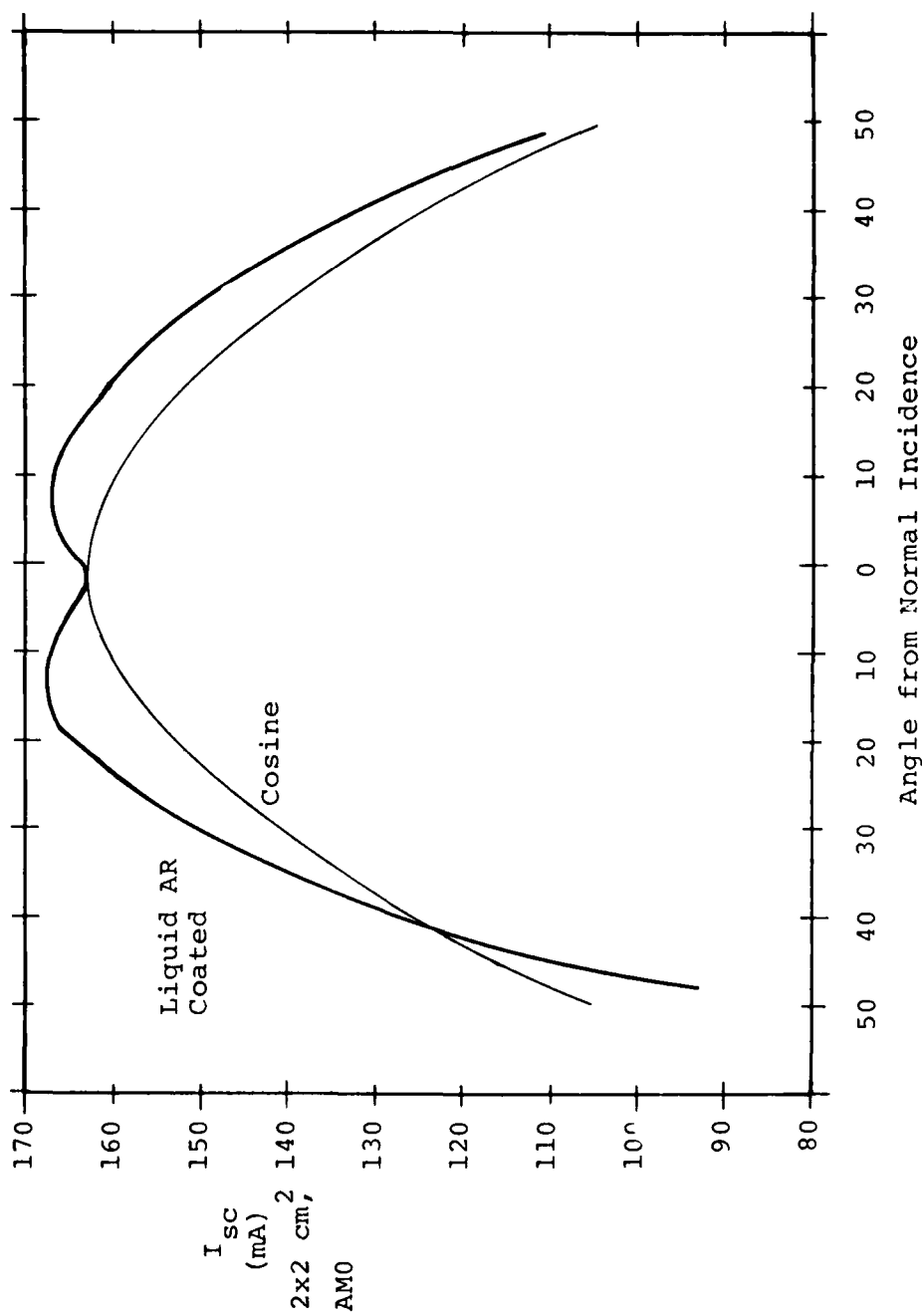


Figure 13. Angular Dependence of Short Circuit Current for Liquid AR Coatings

current (Figure 14), indicating that thick layers of the AR coating are not transparent.

d. Double-Layer AR Coatings

Double-layer AR coatings can be utilized to further reduce reflection from the silicon surface. With the proper choice of materials, a double-layer AR coating can reduce reflection so that less than 2% of the potential current is lost due to reflection. Increases in current of up to 5% above single-layer-coated cells have been observed for cells using double layers of TiO_x and MgF_2 or Ta_2O_5 and MgF_2 . Figure 15 shows reflection versus wavelength for a single-layer and double-layer AR coating on a VJ cell. All of the highest efficiency cells (greater than 14.5%) have employed double-layer AR coatings. At present, TiO_x is the preferred bottom layer because of the voltage problems associated with Ta_2O_5 .

It should be noted that the TiO_x - MgF_2 system is being used as the best match between the silicon and air. The best match for a filtered cell would require two layers with higher index of refraction, namely 2.6 for the bottom layer and 1.7 to 1.8 for the top layer. Future efforts in this area will include the development of better double-layer AR coatings with these indices.

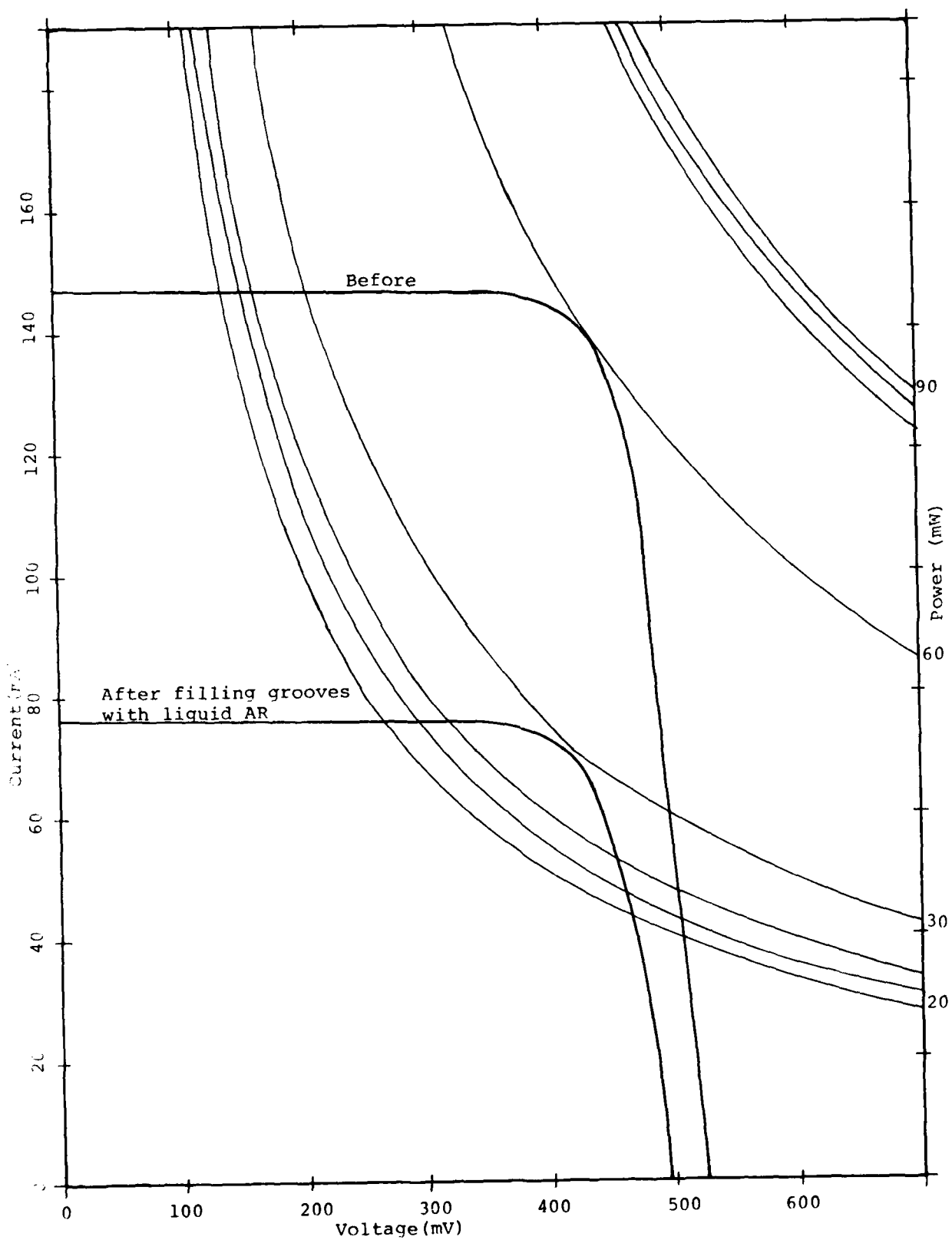


Figure 14. IV Curve Before & After Filling the Grooves with Liquid Ta_2O_5

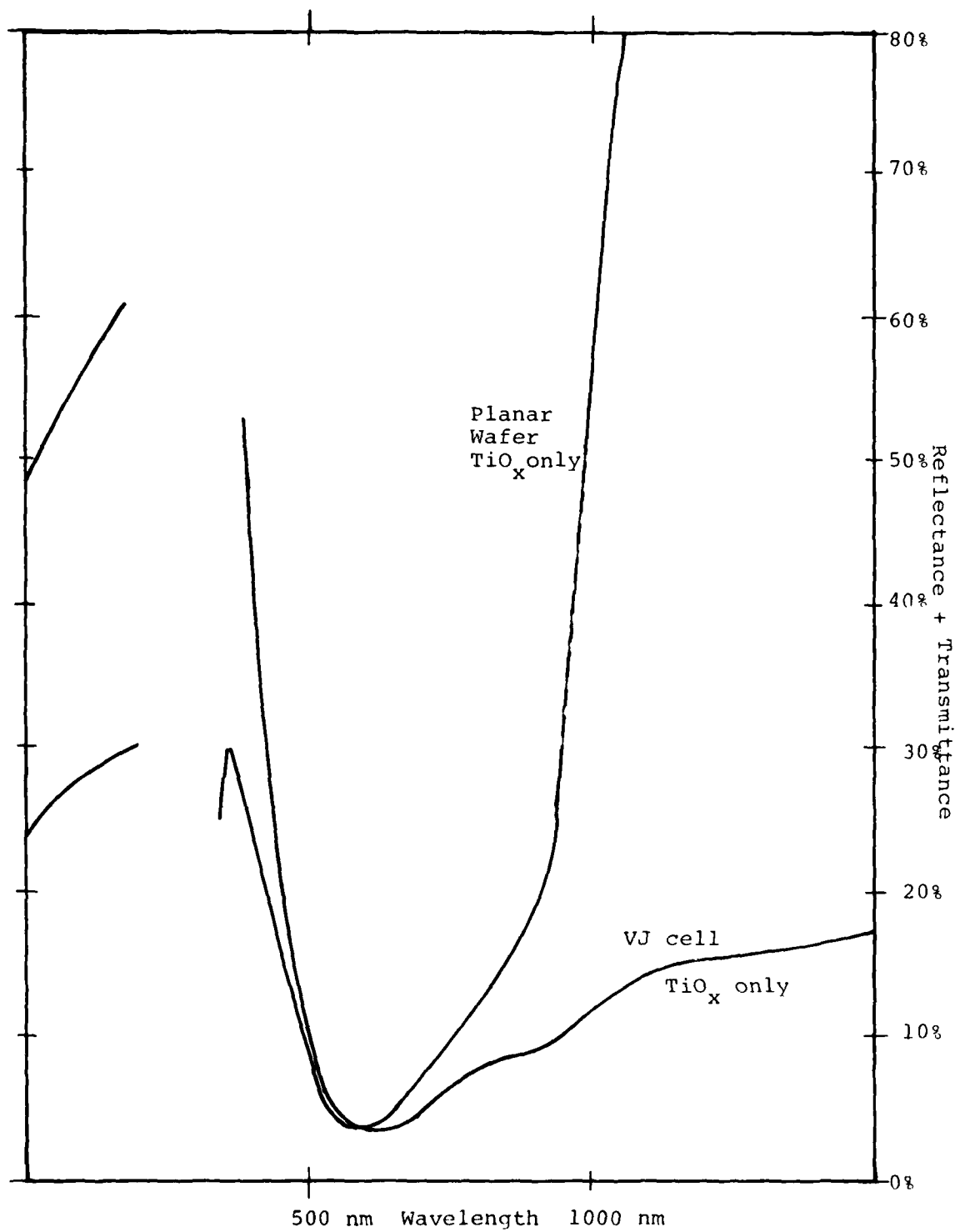


Figure 15. Reflectance vs Wavelength for a Single Layer and Double Layer AR Coating on a VJ Cell

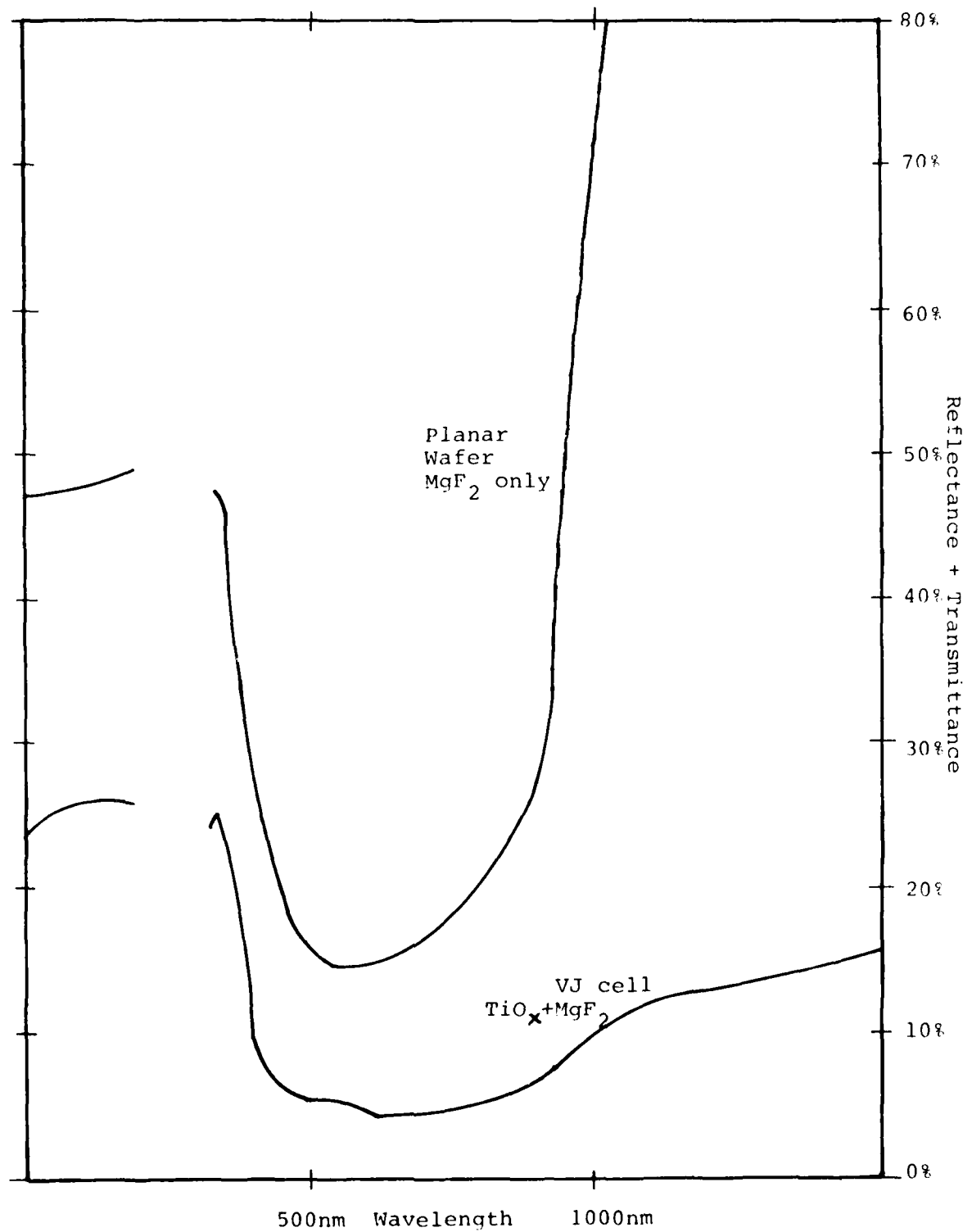


Figure 15. Reflectance vs Wavelength for a Single Layer and Double Layer AR Coating on a VJ Cell

3. RADIATION RESISTANCE

Various VJ cells have been irradiated at NRL using 1 Mev electrons. Figure 16 shows the effect of substrate thickness on radiation resistance for 10 Ω -cm bulk silicon with 25-micron-deep grooves. While the standard-thickness VJ cells are more radiation-resistant than planar cells, the thinner-substrate cells are even more radiation-resistant, with the effect saturating below a 5-mil thickness. As can be seen, this improved radiation resistance is entirely due to the current collection. The VJ cells actually exhibit more decrease in voltage than the planar cells, because the VJ cells have a BSF while the planar cell does not. The increased voltage degradation with increasing thickness indicates that the p^+ itself may be degraded by the irradiation.

VJ cells of both 2 Ω -cm and 10 Ω -cm bulk resistivity have been irradiated (Figure 17). Figure 17 indicates that 10 Ω -cm cells are more radiation-resistant than 2 Ω -cm cells. This data was taken after a 40-hour post-irradiation anneal at 60°C. The cells were also measured before this anneal. The power output of the 2 Ω -cm cells was almost identical to the 10 Ω -cm cells before the anneal, but the 2 Ω -cm cells did not recover after the anneal while the 10 Ω -cm cells did recover significant power. The current of the 10 Ω -cm VJ

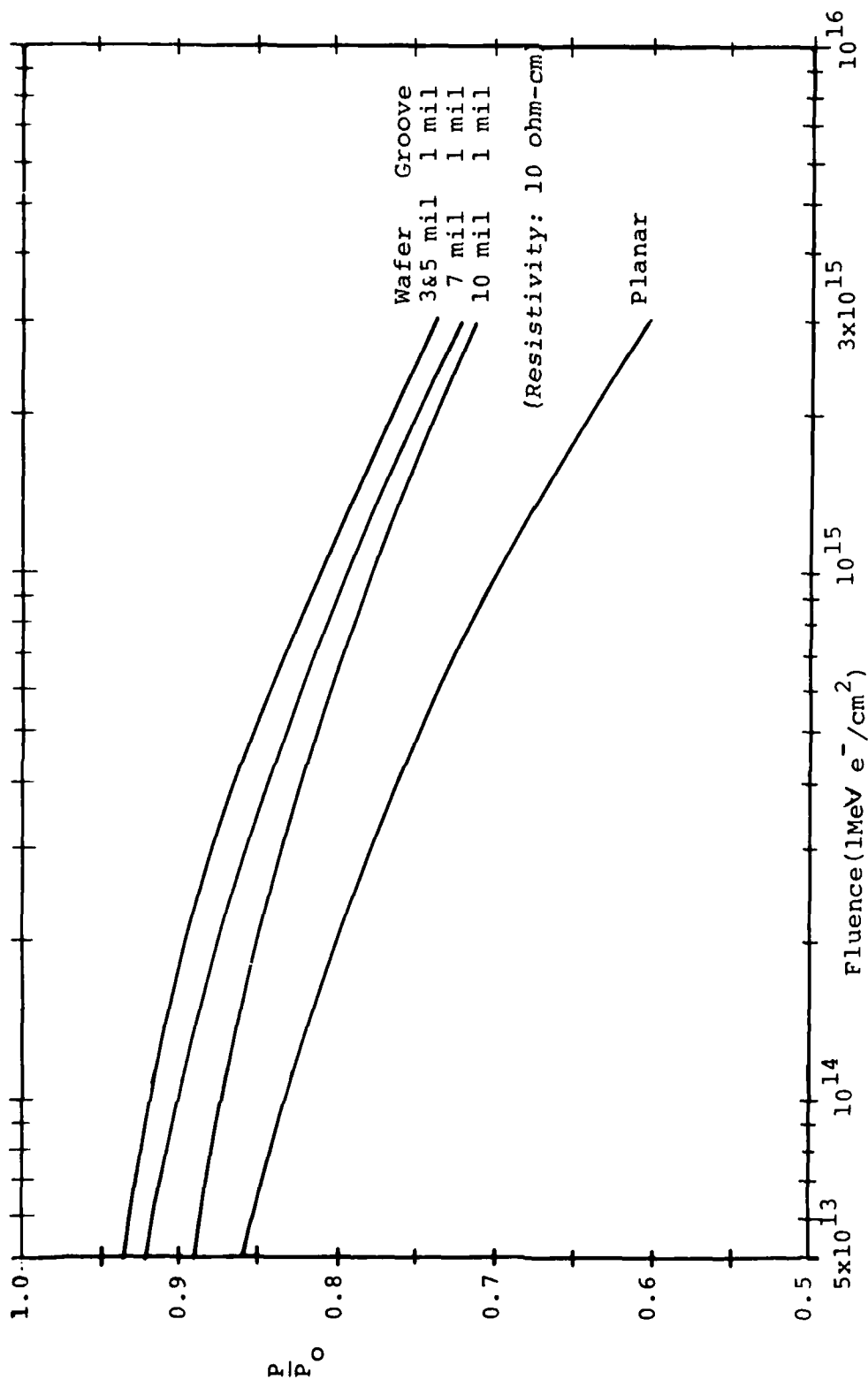


Figure 16a. P/P_0 vs Fluence for Various Substrate Thicknesses

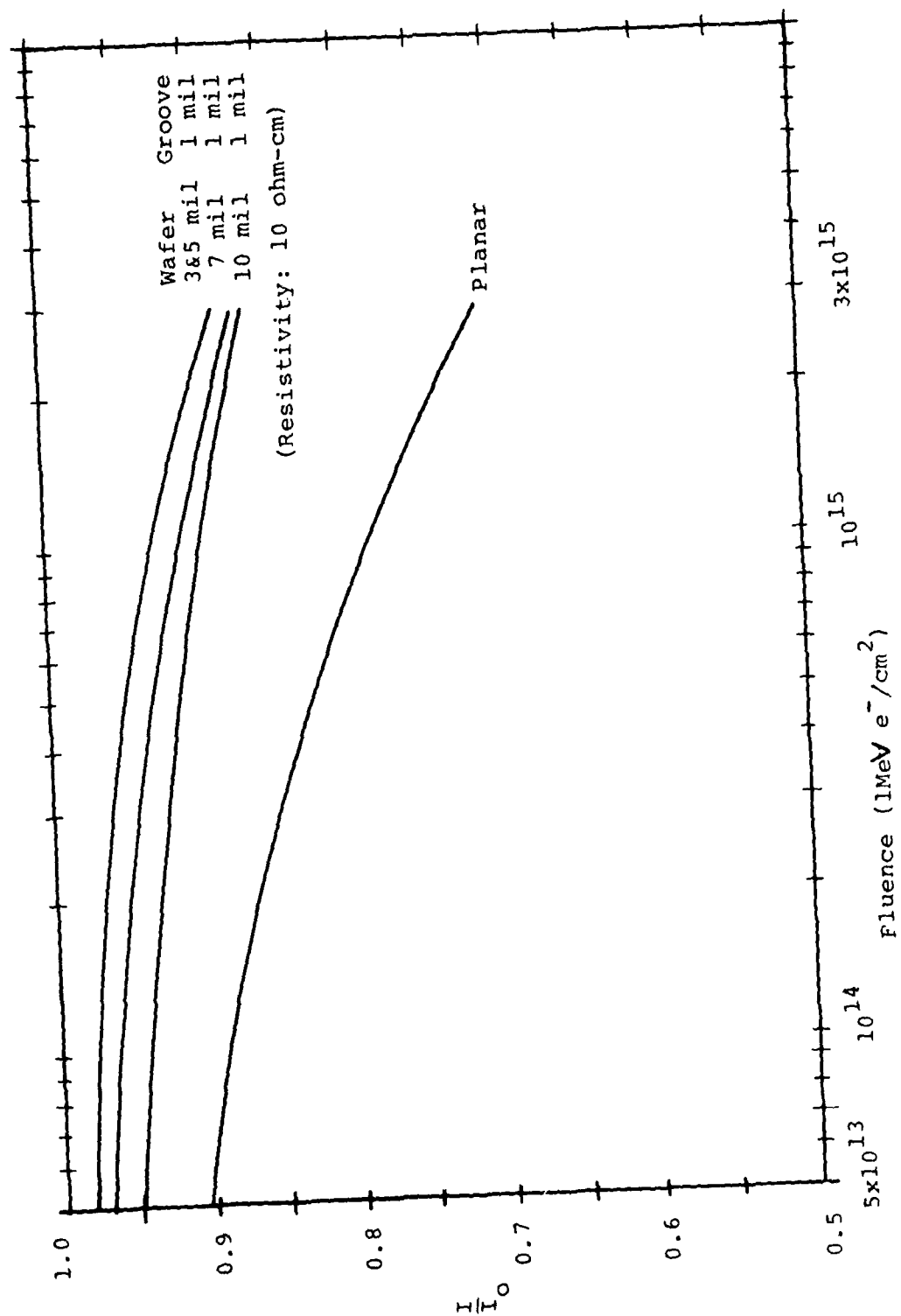


Figure 16b. I_{sc}/I_{sco}

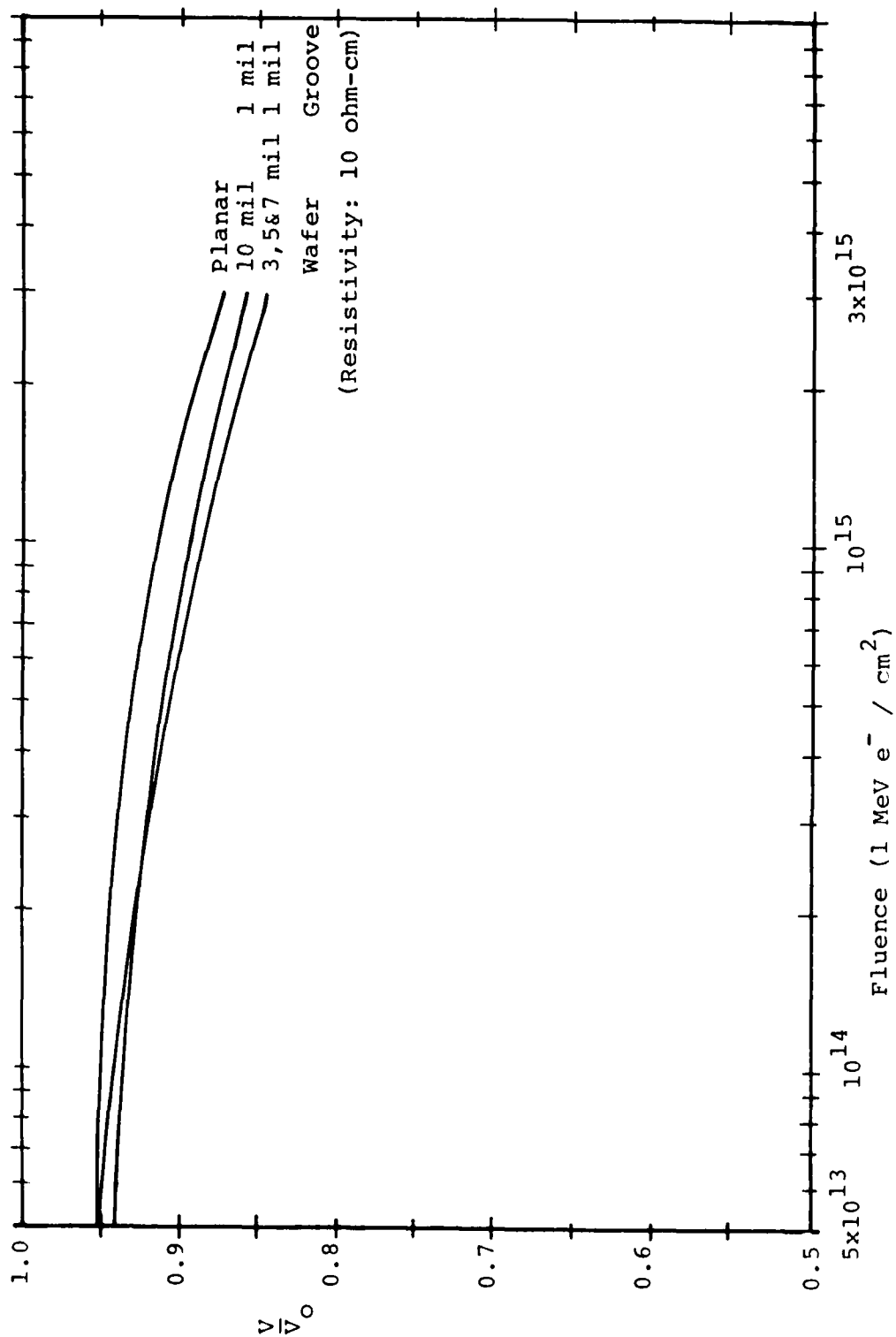


Figure 16c. V_{oc}/V_{oco}

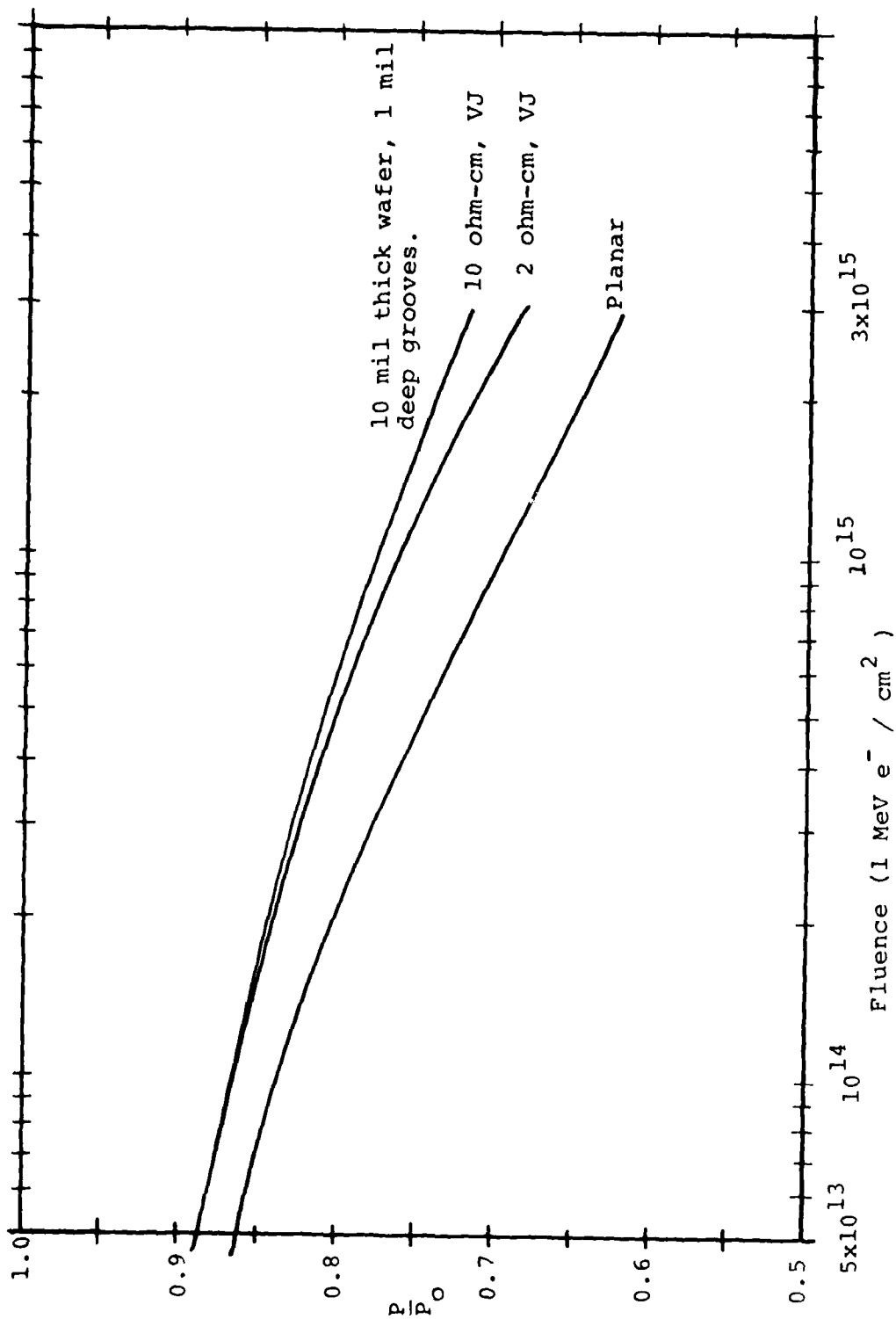


Figure 17a. P/P_0 vs Fluence as a Function of Bulk Resistivity

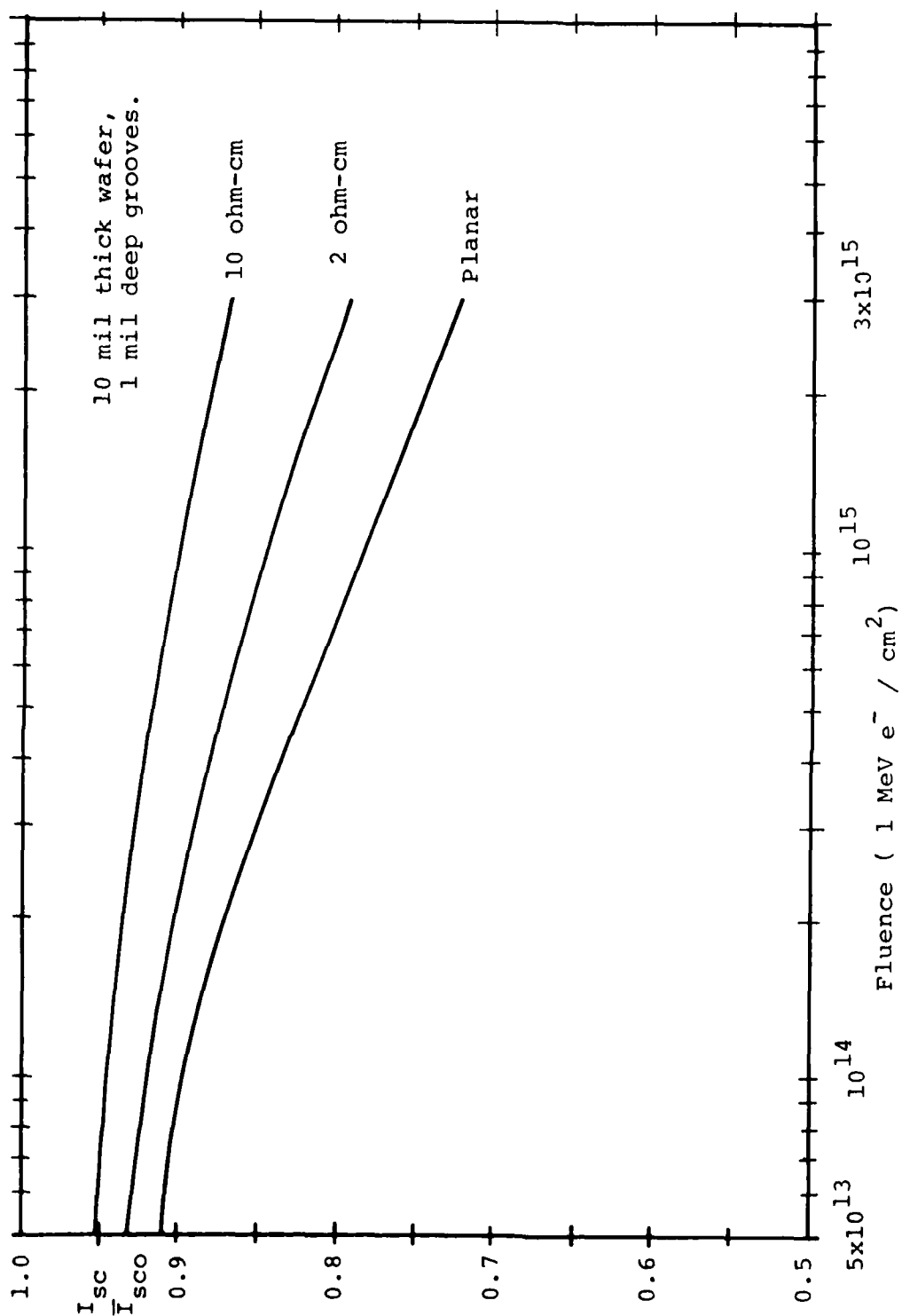


Figure 17b. I_{sc} / I_{sco}

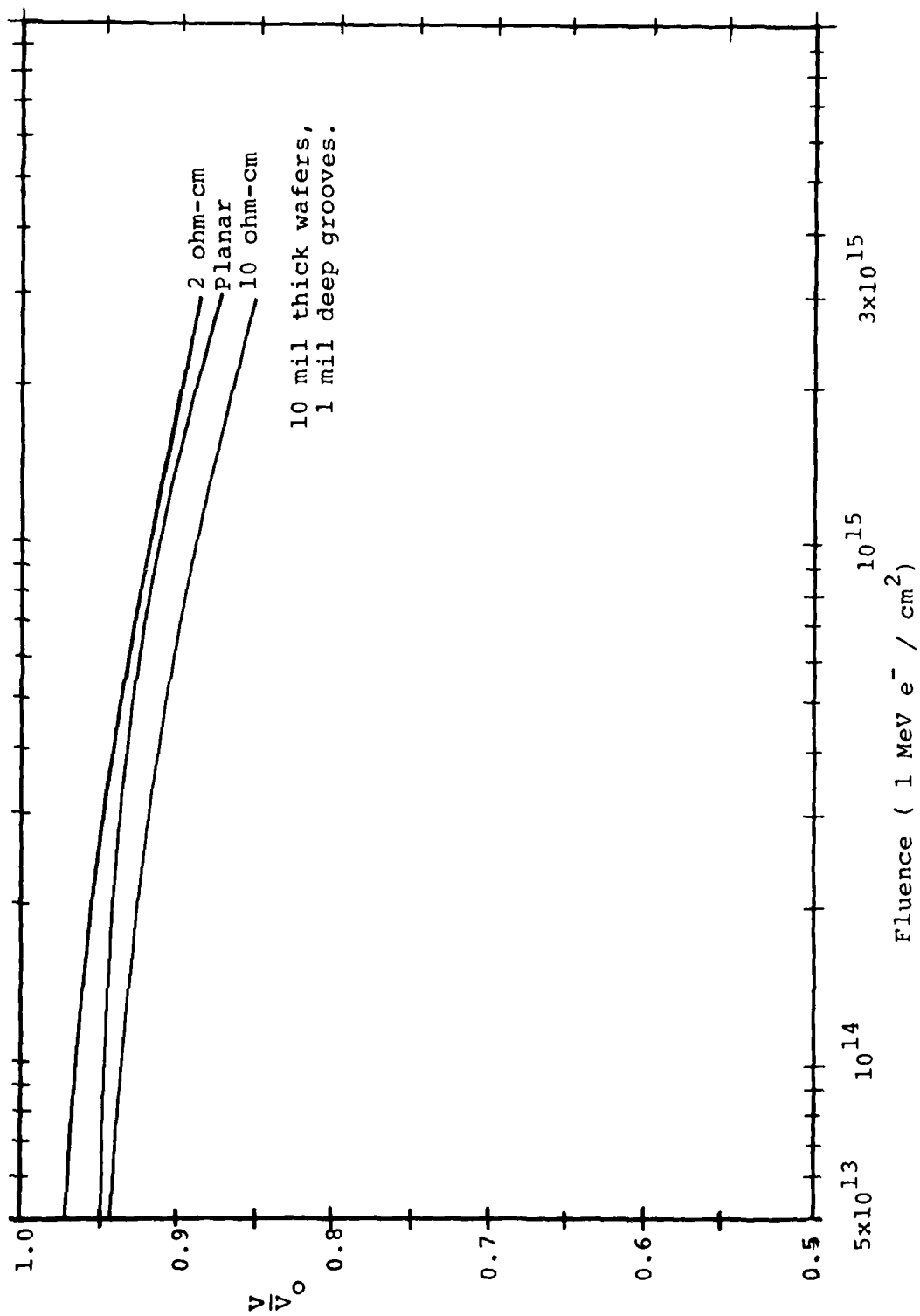


Figure 17c. V_{oc}/V_{oco}

is much more radiation-resistant than the 2 Ω -cm cells, but the situation is reversed for voltage: the 10 Ω -cm cells are less radiation-resistant. The voltage performance of the 2 Ω -cm VJ cell is actually more radiation-resistant than the planar control.

The effect of groove depth on radiation resistance is shown in Figure 18. The deep-groove cells have appreciably better radiation resistance than the shallow-groove cells, although even shallow (25-micron-deep) grooves result in a significant improvement in radiation resistance over planar cells. Most of the increased radiation resistance of deep-groove cells is due to current collection. The voltage, however, of 2 Ω -cm VJ cells is also more radiation-resistant with increasing groove depth. Figure 19 shows that a thin, shallow-groove VJ cell using 10 Ω -cm silicon is nearly as radiation resistant as a thicker deep-groove VJ cell using 2 Ω -cm silicon. Therefore, by proper choice of structure it may be possible to tailor a VJ cell's design to the particular mission.

4. OPTICAL CHARACTERISTICS

The vertical junction structure results in a higher absorptance and emittance than seen for planar cells. Table 7 summarizes the results of such measurements on new-geometry cells with 25-, 50- and 75-micron deep grooves.

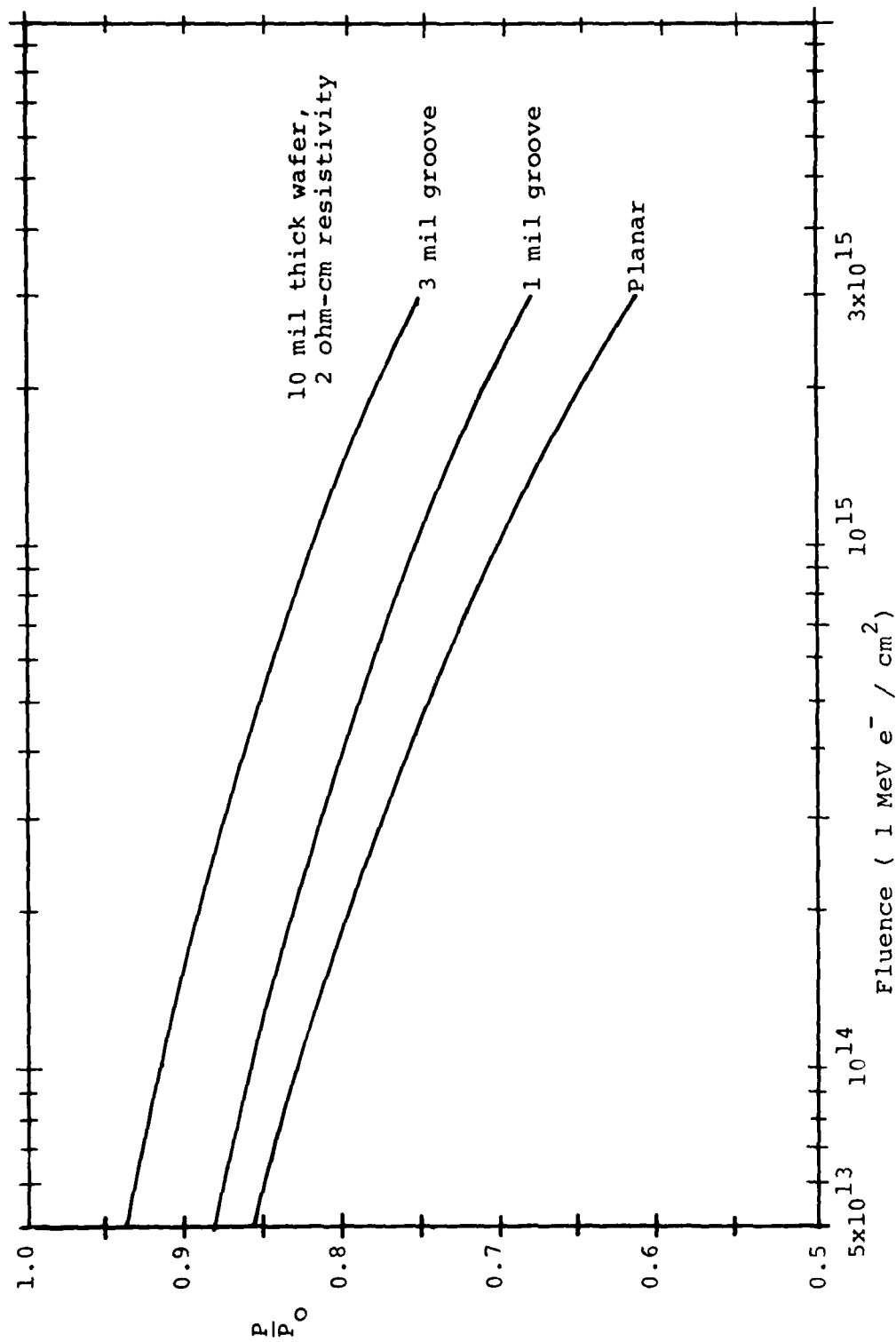


Figure 18a. P/P_0 vs Fluence as a Function of Groove Depth

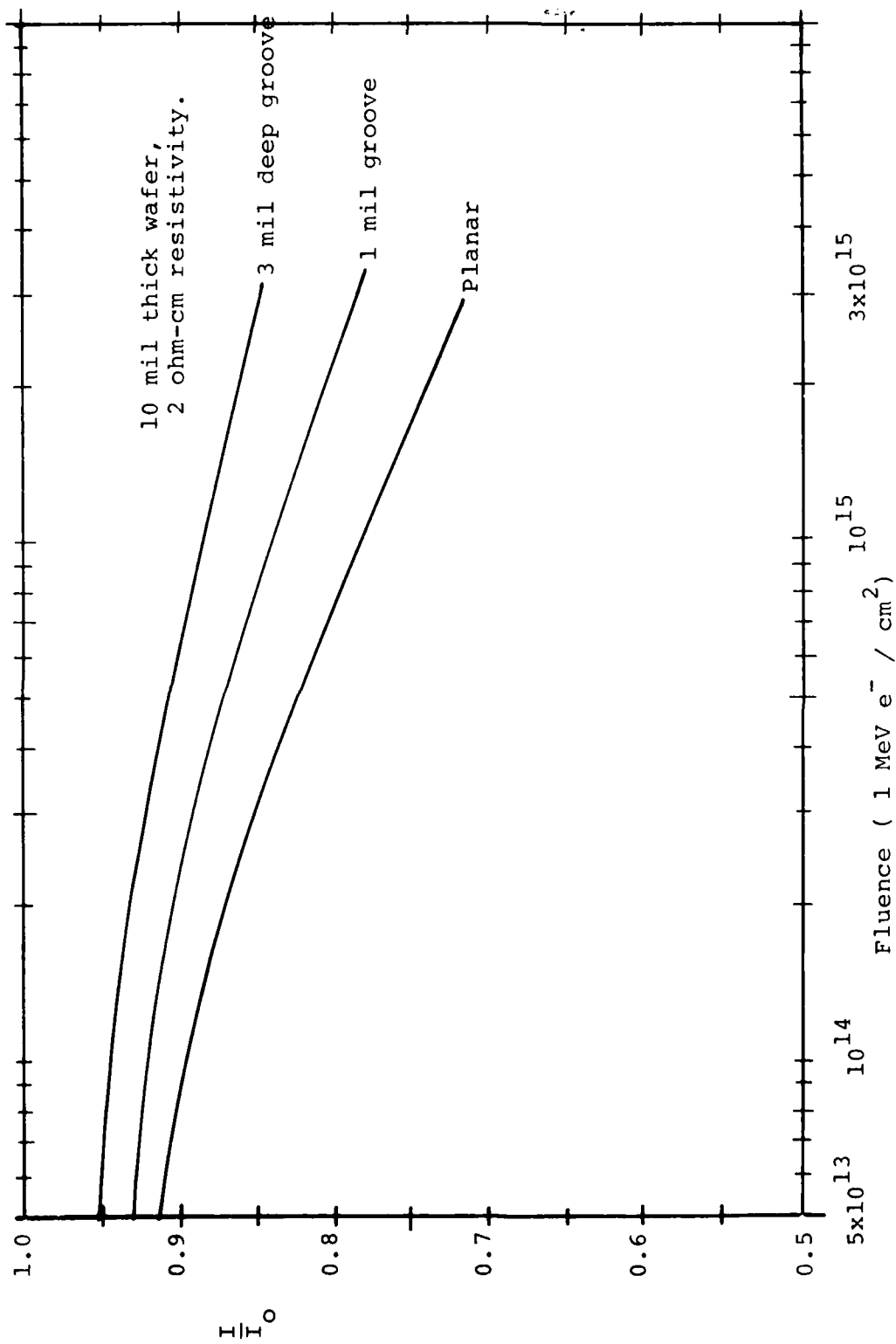


Figure 18b. I_{sc}/I_{sco}

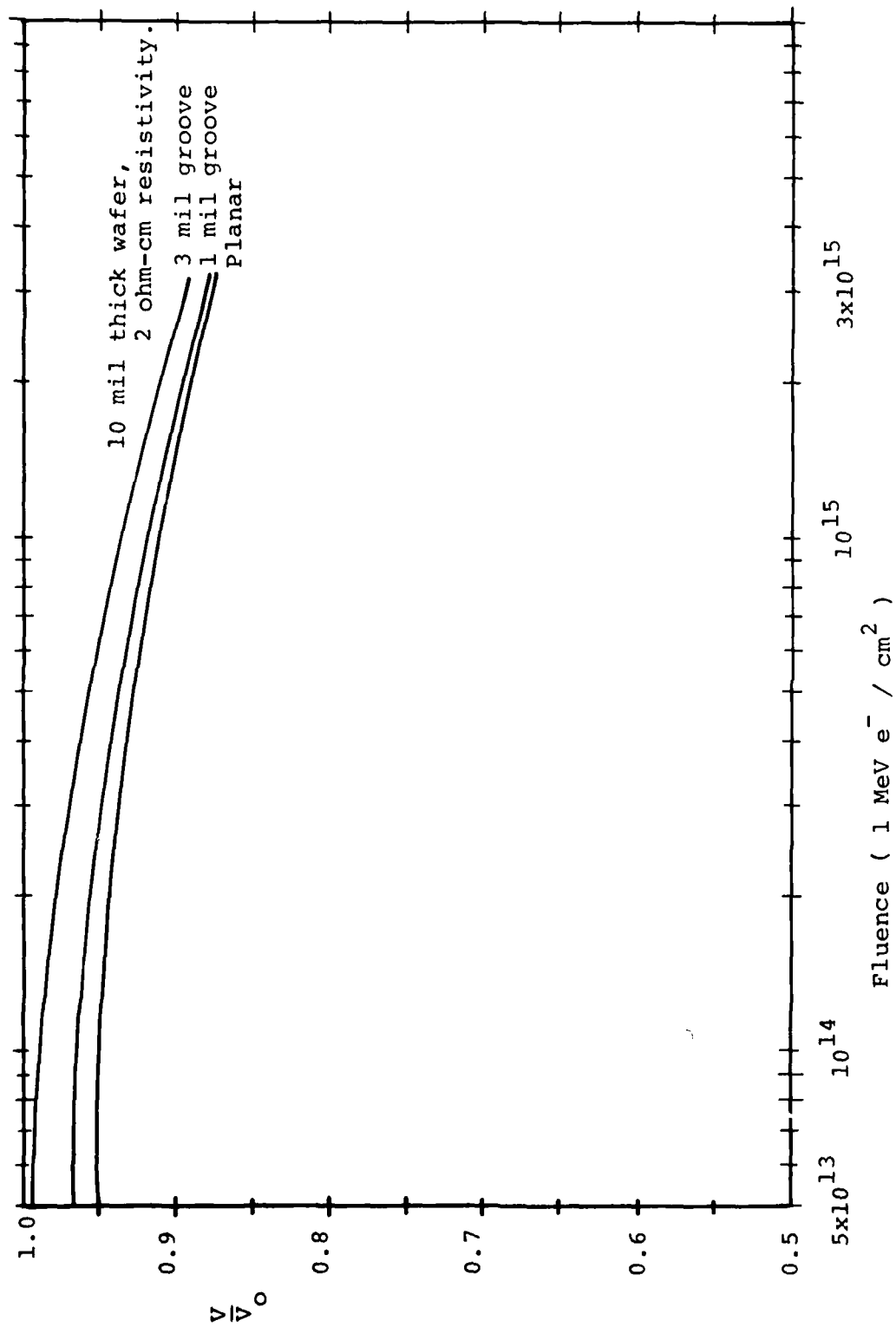


Figure 18c. V_{oc} / V_{oco}

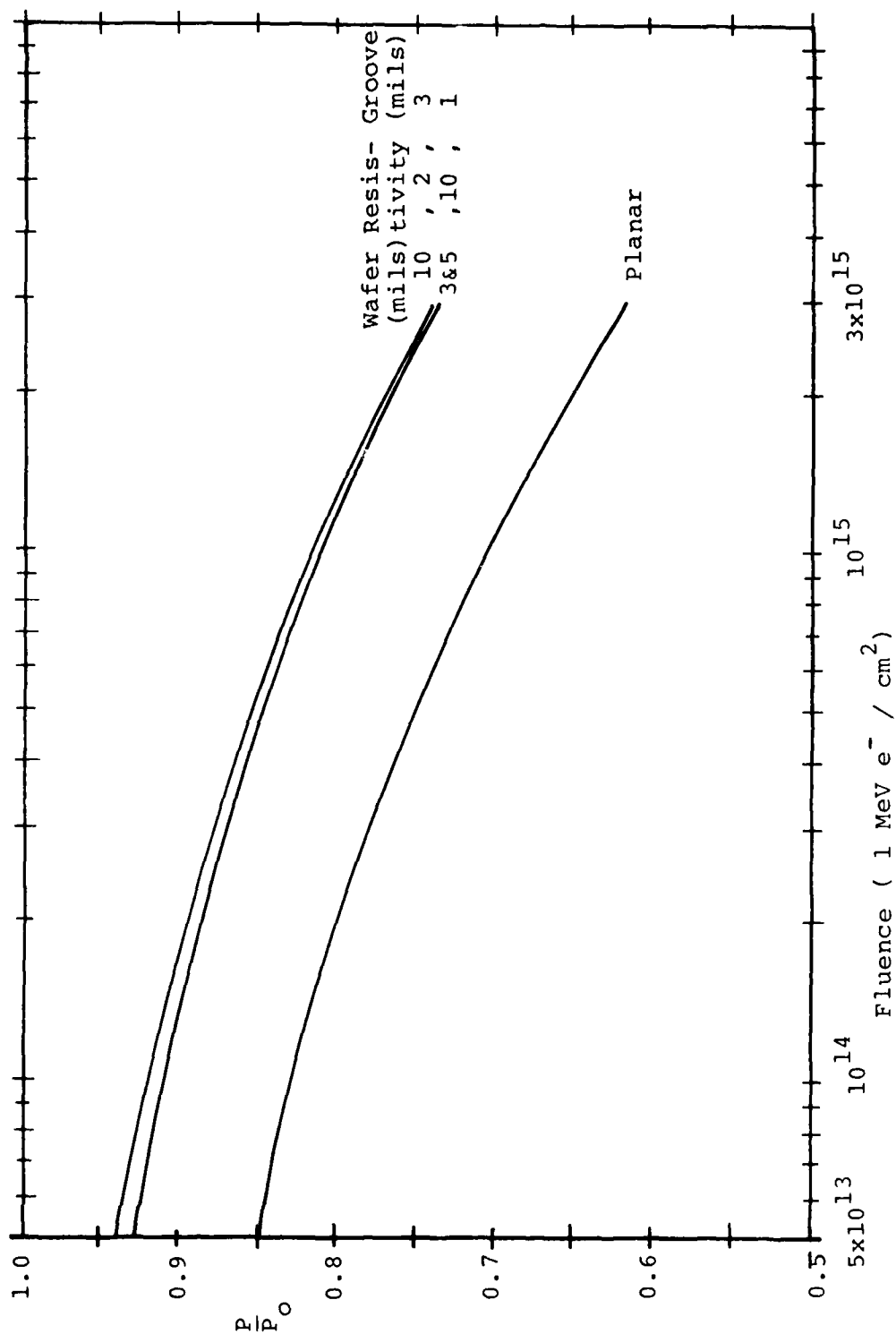


Figure 19. P/P_O vs Fluence for a Thin Shallow-Groove
 10 ohm-cm VJ Cell, a Thick Deep-Groove
 2 ohm-cm VJ Cell, and a Planar Control 2 ohm-cm Cell.

Table 7

OPTICAL PROPERTIES OF NEW-GEOMETRY CELLS
WITH CERIA-DOPED COVERS

Groove Depth (Microns)	ϵH	α	$\alpha/\epsilon H$
25	0.857	0.921	1.07
50	0.854	0.94	1.10
75	0.854	0.929	1.09

The α/ϵ ratios are typical of those obtained from planar (violet type) cells and are appreciably lower than those obtained from pyramid-textured cells (Reference 7). Therefore, under equivalent deployment conditions the VJ cells will operate at a lower temperature than other high-efficiency textured cells.

5. HIGH-TEMPERATURE CONTACTS

Typically, silicon solar cells for space applications have metallization contacts of Ti-Pd-Ag or Cr-Au-Ag. These contact systems cannot operate at temperatures above 450°C, even for short periods, without penetration of the junction and subsequent loss of fill factor. This temperature limit is quite restrictive in light of present requirements for cells that can have electrostatic bonded covers applied,

can be annealed after radiation damage and can be hardened against laser damage. This section describes our preliminary efforts to develop a cell metallization that can withstand a high-temperature soak at 600°C for 5 minutes in vacuum.

The metal placed in contact with the silicon must not penetrate the surface at 600°C, but must make good electrical and mechanical contact with the silicon. Materials commonly considered for solar cell metallization include Ti, Pd, Cr, Ag, Ni and Cu, but all will penetrate the junction at 600°C. To date, we have identified one material, Ta, that can be used as the material in contact with the silicon without degrading cell characteristics. The Ta provides adequate electrical and mechanical contact to the cell, but only if sintered at temperatures above those usually employed for contact sintering. Our Ta contacts would not pass a tape peel test until the sinter temperature was increased to 600°C. At this temperature a 30-second sinter was sufficient to provide excellent contact adhesion. Ta is easily oxidized at elevated temperatures and so must either be sintered in a vacuum or covered with an inert material during the sinter step.

A primary requirement for the bulk of the metallization is its ability to carry the required current. Ag, Cu, and Au are three of the highest-conductivity materials and will

withstand 600°C without melting. These materials have been investigated; each offers some distinct advantages and disadvantages.

Ag

Advantages:

- Highest conductivity
- Easy to solder or weld
- Vast experience in its use for space cells

Disadvantages:

- At 600°C Ag cracks and flows due to surface tension. Experiments in both air and vacuum at 600°C result in both vacuum-evaporated and electroplated silver cracking and forming localized mounds. This phenomenon has been observed with silver deposited directly on Si or deposited on layers of Ta, Ti, Pd and Ti-Pd beneath it on the Si surface.

Cu

Advantages:

- Second highest conductivity (only 5% less than silver)
- Inexpensive
- Easy to solder or weld
- Does not deform or flow at 600°C

Disadvantages:

- Easily oxidizes
- Penetrates a thin layer of Ta at 600°C

Au

Advantages:

- Extremely inert -- humidity- and oxidation-resistant
- Very high melting temperature
- Easy to bond

Disadvantages:

- Lower conductivity (only 2/3 that of Ag)
- High cost. Plating Au onto a 2 cm x 2 cm cell costs approximately \$0.87 per cell (compared to a metallization cost of \$0.18 per 2 x 2 cm cell for Ti-Pd-Ag).

Future efforts are geared to developing Cu and Au as viable contact materials. To use copper, an adequate barrier between the Cu and Si must be found; for Au, an adequate transition material between Ta and Au must be found that can be Au plated.

SECTION 5

CONCLUSIONS

Vertical-junction solar cells have now been fabricated with efficiencies nearly as high as any other silicon solar cell (15%). Their enhanced radiation resistance means that VJ cells are now the silicon cell with the best end-of-life efficiencies available. The fabrication of VJ cells with thin substrates shows that lightweight radiation-resistant arrays can be made using these cells.

Future work on this program will include:

- Research and development on cell fabrication and design to increase the cell efficiency.
- Development of the computer model to correctly understand the optical coupling and BSF operation.
- Testing of the various VJ structures to provide more information on the mechanisms limiting performance.

The intermediate program goal of 16% AM0 efficiency is within reach in a short time frame. The near-term efforts designed to reach this goal are:

- The use of a higher-index double-layer AR coating to improve optical absorption.
- The incorporation of a back surface reflector to improve long wavelength response.
- The use of additives in the Al paste to improve the voltage.
- The redesign of the metallization pattern for shallow-groove cells to minimize series resistance losses in the n^+ region.

These modifications are straightforward and will be implemented in the near future.

The goal of 18% AMO efficiency has not yet been achieved by any silicon solar cell. Techniques we plan to implement in reaching for this goal include:

- Ion implantation and subsequent anneal to provide a more uniform doping density (for both n^+ and p^+ region).
- Oxidation of the n^+ surface to reduce the front surface recombination velocity.
- Texturing of the VJ surface to improve the optical absorption.

- Use of higher-purity starting silicon to take advantage of a longer diffusion length.

These efforts are more highly speculative than those required to reach to 16% goal. Any or all of them may not prove effective or may be too costly, but each will be assessed during the latter stages of the program.

REFERENCES

1. J. Wohlgemuth, J. Lindmayer, and A. Scheinine, Non-Reflecting Vertical Junction Silicon Solar Cell Optimization. Technical Report AFAPL-TR-77-30, July 1977.
2. J. H. Wohlgemuth and C. Y. Wrigley, Non-Reflecting Vertical Junction Silicon Solar Cell Optimization. Technical Report AFAPL-TR-78-81, November 1978.
3. J. H. Wohlgemuth, C. Y. Wrigley, and J. Lindmayer, Vertical Junction Solar Cell. Proceedings of Thirteenth Intersociety Energy Conversion Engineering Conference. San Diego, California, 1978, p. 80.
4. W. W. Lloyd, R. Yeakley, C. Fuller, and F. Malone, Development of Vertical Multijunction Solar Cells for Spacecraft Primary Power. Technical Report AFAPL-TR-74-45, Vol. II, June 1975.
5. D. L. Kendal, On Etching Very Narrow Grooves in Silicon. Applied Physics Letters, 26, February 1975, pp. 195-198.
6. M. Mendel and K. Yong, Polishing of Silicon by the Cupric Ion Process. Proceedings of the IEEE, 50, Sept. 1969, pp. 1476-1480.
7. A. Meulenber, D. J. Curtin and R. W. Cool: Comparative Testing of High Efficiency Silicon Solar Cells. Twelfth IEEE Photovoltaic Specialists Conference, 1977, pp. 238-246.